J. ISSS Vol. 3 No. 1, pp. 28-77, March 2014.
REVIEW ARTICLE

Nanotextile Bio-sensors for Mobile Wireless Wearable Health Monitoring of Neurological and Cardiovascular Disorders

Pratyush Rai[1], Sechang Oh[1], Prashanth Shyamkumar[1], Mouli Ramasamy[1], Robert E. Harbaugh[4] and Vijay K. Varadan[1,2,3,4]

[1]Department of Electrical Engineering, University of Arkansas, Fayetteville, AR 72701
[2]Department of Biomedical Engineering, University of Arkansas, Fayetteville, AR 72701
[3]Global Institute of Nanotechnology, 700 Research Center Blvd, Fayetteville, AR 72701
[4]Department of Neurosurgery,
Pennsylvania State University, Hershey, PA 17033
Corresponding Author: vjvesm@uark.edu

Keywords:

Textile nanosensor,
smart textile,
wireless, bioelectromagnetism,
ECG, EEG, EOG, EMG,
cardiovascular disorder,
neurological disorder

Abstract

Health and long term care is a growth area for wearable heath monitoring systems. Wearable diagnostic and therapeutic systems can contribute to timely point-of-care for patients with chronic health conditions, especially chronic neurological disorders, cardiovascular diseases and strokes that are leading causes of mortality worldwide. Diagnostics and therapeutics for patients under timely point-of-care can save thousands of lives. However, lack of access to minimally-intrusive monitoring systems makes timely diagnosis difficult and sometimes impossible. Existing ambulatory recording equipment are incapable of performing continuous remote patient monitoring because of the inability of conventional silver-silver-chloride-gel-electrodes to perform long-term monitoring, non-reusability, lack of scalable-standardized wireless communication platforms, and user-friendly design. Recent progress in nanotextile biosensors and mobile platforms has resulted in novel wearable health monitoring systems for neurological and cardiovascular disorders. This chapter discusses nanostructured-textile-based dry electrodes that are better suited for long-term measurement of electrocardiography (ECG), electroencephalography (EEG), electrooculography (EOG), electromyography (EMG) and bioimpedance with very low baseline noise, improved sensitivity and seamless integration into garments of daily use. It discusses the bioelectromagnetic principles of the origin and propagation of bioelectric signals and nanosensor functioning, which provide a unique perspective on the development of novel wearable systems that harness their potential. Combined with state-of-the-art embedded wireless network devices to communicate with smartphones, laptops or directly to remote servers through a mobile network (GSM,4G-LTE,GPRS), they can function as wearable wireless health- diagnostic systems that are more intuitive to use.

1. Introduction

Public spending on health and long term care in Organization for Economic Co-operation and Development (OECD) member countries and BRIICS (Brazil, Russia, India, Indonesia, China, South Africa) is 6% of the GDP and is projected to increase up to 14% in the next 50 years [de la Maisonneuve *et al.*, 2013]. Chronic disease diagnosis and treatment are the primary causes for this increase. Patients suffering from chronic diseases need to repeatedly visit one hospital, which can be expensive. As a solution to this, remote Point-of-Care (POC) systems and Remote Patient Monitoring (RPM) systems can be used. Remote patient monitoring for point-of-care facilitates the monitoring of a patient's health condition at local or remote places without the need for hospital admissions or visits. In the case of high risk patients, it can provide the patient with real time feedback from a medical center.

Wearable nanosensor systems in the form of smart clothing, equipped with wireless communication technology, provide real-time medical data to health professionals for early diagnosis, planning therapeutic intervention and following up on the effect of planned therapy. Techniques such as electrocardiography (ECG), electroencephalography (EEG), electrooculography (EOG), electromyography (EMG) and electrical impedance tomography are relevant to POC for cardiovascular disease, neurological disorders, cancer and strokes.

Intelligent wearable sensor systems with simple installation, minimal maintenance and user involvement can be the best method for ubiquitous health monitoring. They combine the high sensitivity of nanosensors with cost effective and lightweight textiles. Long term real-time health monitoring is useful in chronic diseases for event detection, onset of critical episodes, and disease management through diagnostics and therapeutics [CDC, 2013]. Unobtrusive wearable health monitoring is found to be effective in the prevention and early diagnosis of neurological and cardiovascular disease by non-invasively monitoring a person's vital signs and physiological data [Jorg, 2003].

In this chapter, nanotextile-based wireless biosensor systems have been described. Over the past few decades, advancements in pervasive information and communication technologies, coupled with microelectronics and systems development have provided an opportunity for the integration of electronics with functional textiles. The confluence of these two fields has radically transformed the norms of computing and embedded systems into soft textile interfaces [Marculescu *et al.*, 2003]. In the section on *Smart textile for health monitoring*, the concept of a textile as a health monitoring platform is explained along with a discussion on newly developed nano and micro scale fiber structures, composite materials and coatings that integrate with textile fabrics to create *smart textiles*. The Section on *Electrical signals from brain and heart* offers a brief development of the prevalent models used to describe the relationship between the activity of a single neural cell or cardiac myocyte and the characteristic bioelectric signals measured at the level of the skin-electrode interface (EEG, ECG, EOG and EMG), and a comparison between planar textile electrodes and nanostructured electrodes. In the section on *Monitoring and Diagnosis*, we describe the bioelectric signals of diagnostic value for both neurological and cardiological disorders.

The section on *monitoring systems* talks about the different types of wireless protocols that are used in the current state –of the- art for wireless sensor systems. Finally, in the sections *Neurological Disorder monitoring by Wearable Wireless Nano- Bio- Textile sensors*, *Cardiovascular Health Monitoring* and *Biofeedback system for therapeutics*, numerous applications have been showcased to demonstrate the cutting edge of textile-based wearable health monitoring technology for neurological and cardiovascular health disorders.

2. Smart textiles for Health Monitoring

Current technologies for measuring and recording biopotential signals discussed in the section on *Monitoring systems* are suitable for bedside monitoring, with the exception of the Holter monitor. POC diagnostics and therapeutics require systems capable of ambulatory and/or remote monitoring. Such systems will allow patients and high risk individuals to stay in their homes and follow their routine, while the continuous monitoring of their

neural and/or cardiac functions can be performed remotely. The key to the successful adoption of remote health care is invisibility, i.e. sensors that do not interfere with the quotidian activities of the individuals, and, at the same time, efficiently monitor parameters critical to neural and cardiac health.

2.1 Textile Platform for Nano- biosensors

Textile based sensor systems are flexible sensors that are made of textiles or have the suitable texture and flexibility to embed or integrate into textiles of daily use. The resultant functionalized textiles are called e-textiles or smart textiles. They are distinct from wearable computing systems because they emphasize the seamless integration of the textiles with sensors and sensor electronics. Textiles are preferred for the integration of biomedical sensors because they are the most natural materials to use next to the human body. Thus, they facilitate unobtrusive observation, where they simply sense and record the physiological signals of the subject without any kind of active interaction with the subject.

Textile based nano-biosensor systems can be integrated with compact textile integrated wireless electronics, with the help of woven or printed connections, for remote wireless health diagnostics [Rai *et al*., 2012]. It eliminates the use of stick on glue based electrodes and can be worn without the help of medical personnel; therefore, it is a desirable diagnostic system in hospitals as well as in remote locations.

Smart textiles have been an area of focus for space exploration, biomedical and consumer electronics communities for their potential to significantly augment the Body Area Network (BAN) which is also known as the internet of things [Bergey *et al*., 1971; David *et al*., 1972; Khosla, 2012]. Xiaoming Tao describes Smart Textiles as a class of smart materials and structures that sense and react to environmental conditions or stimuli. Smart textiles can be divided into three subcategories. Passive smart textiles can only sense environmental conditions and stimuli. Active smart textiles can sense and react to environmental conditions and stimuli. Very smart textiles can sense, react and adapt to environmental conditions and stimuli. In addition to these types, intelligent textiles can cause predictable effects or phenomena by interacting with the environment and the wearer [Tao, 2000; Zhang, 2001; Pejis, 2005]. By this definition, nanotextile- based wireless biosensor systems are wearable smart nanosystems.

The Smallest units of the textile are fibres or filaments. Innumerable combinations of these units can result in many textile materials with varying length, cross-sectional areas and shapes, and surface roughness. The intelligent functionality can be introduced into the textile at different levels. At the fibre level, a coating can be applied or threads can be added to make a composite textile. The Fibres of different types can be arranged at random or in a strictly organized way in yarns or fabric to form even 3D structures. These structures can be metallized or functionalized to fabricate a conductive textile electrode and other functional surfaces with micro or nanorod, micro or nanocoil arrays.

Smart textiles (fabric) can be made from materials ranging from traditional cotton, polyester and nylon to advanced Kevlar with integrated functionalities. However, in the scope of the present review, fabrics with electrical conductivity are of interest. There are two kinds of smart textiles (fabric) products that have been developed and studied for health monitoring fabrics with textile-based sensor electronics [Park *et al.,* 1999; Park *et al.,* 2007; Coosemans *et al.,* 2006; Lee *et al.,* 2009; Alzadi *et al.,* 2012] and fabrics that envelop traditional sensor electronics [Trainer, Smartex]. Pioneering research work, done by Jayaraman and co-workers, showed that weaving can be used to incorporate electrically conductive yarn into the fabric to obtain a textile that can be used as a "Wearable Motherboard". It can connect multiple sensors on the body, such as wet gel ECG electrodes, to the signal acquisition electronics [Park *et al.,* 1999; Park *et al.,* 2007]. Later researchers have shown that conductive yarns can be instrumental in the fabrication 4 of textile- based sensors made of fabric [Coosemans *et al.,* 2006; Lee. Y *et al.,* 2009] or metallic meshes [Alzadi *et al.,* 2012] coated with silver or conductive metal cores woven into the fabric [Rattfalt *et al.,* 2007].

2.2 Nanostructured Textile

Naturally occurring fibers have diameters in the order of microns, and the smallest diameter is of silk fibers (10μm). It is a common conception

that textiles made of fibers with diameters in the nanometer scale can be deemed the textiles fit for nanosensor applications. These textiles, integrated into the fabric, can serve as different components of smart sensor systems.

Based on the degree of integration, the combination of electronics and textiles can be divided into embedded electronics, textronics and fiberonics 5. Embedded electronics uses textiles as a platform for building in readily available off-the-shelf electronics (e.g., Phillips illuminative LED shirts and Lifeshirt by VivoMetrics [Aarts *et al.*, 2003]). These can be nanosensor chips made with state of the art nanofabrication techniques. In such smart textiles, the electronics have to be disconnected prior to washing because they cannot endure washing.

Textronics uses electronic components manufactured by using textile materials and textile production techniques. Nanocomposites and nanoparticles can be incorporated in to the textile to form sensitive layers and sensor connects. Mazzoldi et al and De Rossi et al have developed polypyrrole on Lycra and carbon-filled6 rubber based printable sensors for the measurement of posture, movement and respiration. These textronics based suits have been demonstrated for monitoring rehabilitation, studying ergonomics, virtual reality and ambulatory monitoring [Mazzoldi *et al.*, 2002; De Rossi *et al.*, 2003]. Due to the limitation of materials and fabrication techniques, complex electronic components such as microprocessors, cannot be fabricated as textronics and should still be embedded in textiles. The research done by Clemens *et al*. [Clemens *et al.*, 2003] attempts to integrate basic electronic building blocks, such as semiconductor electronics, in yarns for the fabrication of transistors on textile. This fiberonics technology can help in the full inclusion of microprocessors and nano-biosensors in future textiles.

Textronics has the potential for creating textiles with new attributes, while keeping them flexible and washable. For textronic technology, knowledge of and access to textile production is necessary. There are many textile production techniques that can be used to build electronic components. A commonly-used concept for making textile-based sensors and electronics is weaving or knitting conductive thread into the garment fabric. Jacquard loop weaving can weave conductive yarn into specific patterns for making conductive tracks, contacts and antennas [Gimpel, *et al.*, 2004]. Plain and circular knitting, warp knitting or crocheting can be used for the knitting of conductive yarns into textile electrodes and strain sensors (e.g. GOW trainer [GOW Trainer], Numetrex by Adidas [Jorg, 2003, Numetrex], Wearable Wellness System from Smartex s.r.l. Pisa Italy [Smartex]). The Embroidery of conductive yarns into textiles can be useful in making wearable keyboards [Post *et al.*, 1997] and antennas [Catrysse, 2004].

2.3 Nanotextured Textiles as Electronic Sensors

Smart textiles can serve as a platform for electrophysiological sensors that require being in contact with the body. Studies have shown that textile-based sensor electrodes are as reliable as conventional silver-silver chloride gel-based electrodes for the detection of ECG signals [Rai *et al*., 2012; Pantelopoulos *et al.*, 2008; Pacelli, 2006].

Textiles as substrates can support nanostructures grown on them [Lim, 2010], embedded as composite [Vigneshwaran *et al.*, 2006], embedded/mounted as nanomaterials based devices [Dhawan *et al.*, 2006; Varadan *et al.*, 2010; Varadan *et al.*, 2011] or nanomaterials-based coating and dyes [Maharani *et al.*, 2010; Locher *et al.*, 2006]. Conductive fabrics can be obtained by weaving conductive yarn into fabrics [Dhawan *et al.*, 2004], coating conductive layers on a fabric surface by chemical processes such as polymerization [Xue *et al.*, 2005], electroless plating [Jiang *et al.*, 2006] electroplating [Brenov et al 2006], or physical processes such as vacuum sputter deposition [Wang, 2007; Yeon, 2004]. The Incorporation of nanofibers in to the textile is also possible by drawing out nano-filaments using an electrospining technique [Holme, 2005]. Alternatively, pre-extruded nanofibers can be deposited with the help of electrodeposition. In either case, the nanofibers form a mat or a web that renders the textile substrate as nanotextured. These textile surfaces have a large surface area and surface to volume ratio. The large surface area improves the absorption or adsorption property of

the textile substrate to make them useful as sensor layers for gas sensors [Tonezzer *et al.*, 2012], biological sensors [Naik, 2004], chemical sensors [Munirathinam *et al.*, 2013], biomedical textiles [Sahoo *et al.*, 2006], water purifiers [Barhate *et al.*, 2007] and electrodes for biopotential measurement [Oh *et al.*, 2013].

Free-standing aligned nanostructures can be obtained on a textile electrode surface by using the traditional technique of flocking. It uses an electric field or pneumatic force to drive down millions of individual fibers that have a static charge on them. The electric field, in particular, aligns the charged fibers vertically and the static charge ensures that they are apart from each other. The vertically aligned fibers are driven down on to a flexible surface, such as a textile or polymer substrate, and pretreated with adhesive for the fibers to get planted [Rai *et al.*, 2013].Synthetic long chain polymers such as polyester, nylon, polyimide and polyaramid are melt- blown or solution blown, or extruded and spun into fibers on a spinneret. The techniques for drawing out the fibers can be modified to obtain fibers with diameters in the order of nanometers (40-2000 nm). These processes can obtain fibers that are only as wide as the single layer crystal made of polymer chains [Reneker *et al.*, 1996]. The conventional synthetic polymer fiber spinning technology has been improved to produce composite fiber. A mixture of two polymers, that are mutually immiscible, can be drawn in to fibers by extrusion such that one polymer forms long fibers in a matrix of the other. A cross-section of such a fiber shows that 60-1500 islands of one polymer fibers are distributed in a sea of the other polymer, thus giving the impression of islands in the sea [Baker, 1992]. Composite fibers are best suited because they can be flocked as microfibers and then bundled. Island polymer nanofibers can be released by dissolving the sea polymer (Figure 1). This is followed by the metallization of the structures with silver by the electroless plating method.

The surface of sensor electrodes can have nanoscale and mesoscale free- standing conductive structures. This contributes to increasing the effective surface area of the electrodes and high aspect ratio nano/mesoscale structures can overcome the obstruction due to a rough skin surface and body hair (Figure 2). A good skin-

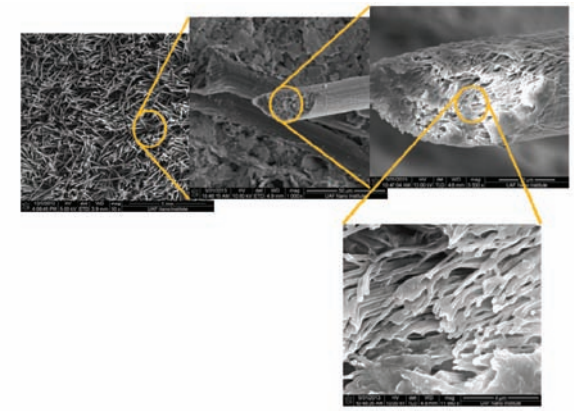

Figure 1 Nanostructured electrode surface

electrode interface with these nanostructured sensor electrodes is instrumental in the detection of electrophysiological signals emanating from the brain and heart to the skin surface. Figure 3 shows that the next step would be to understand the principles behind the signals generated by the brain and heart. This understanding should then be extended to the skin-electrode interface to study the effects of nanostructured sensor electrodes on the monitoring of signals that are important for the diagnosis of neurological and cardiovascular disorders.

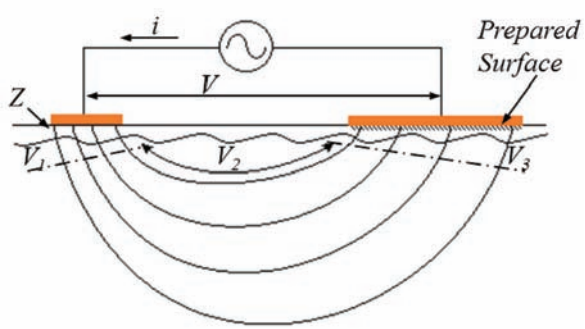

Figure 2 2-electrode configuration for recording skin-electrode impedance (Z) such that Z = V/i because V_1>> V_2, V_3.

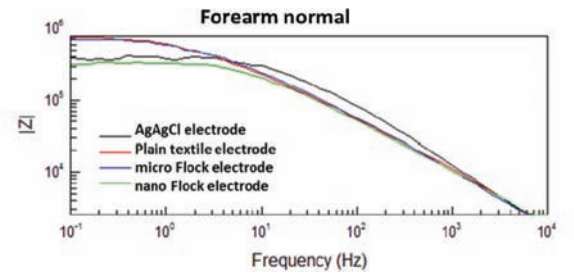

Figure 3 Comparison of impedance spectroscopy on plane textile electrode, microstructured electrode and nanostructured electrode with Ag/AgCl gel electrode as standard. Testing was performed on forearm of young adult.

3. Electrical Signals from Brain and Heart

Nanotextile-based biosensors for EEG, EOG, EMG and ECG detect bioelectromagnetic signals generated by the brain, muscles and heart, while being in contact with the skin. In this section, the bioelectromagnetism involved in the origin and propagation of bioelectric signals of interest i.e. EEG, EOG, EMG and ECG have been presented. This will lay the ground work for an electromagnetic theory of a skin-electrode interface to explain the superiority of nanostructured electrodes over plane and microstructured electrodes, thus, emphasizing the potential for the development of novel systems through a ground-up understanding of the signal sources i.e. neurons of brain tissue and myocytes of heart tissue, respectively.

3.1 Neurological anatomy and electrophysiology

The Brain is the central organ of the nervous system, which reaches every part of the body. It is responsible for sensory functions such as vision, touch, hearing, taste and smell. The Brain is the center of cognitive functions such as logical thinking, speech, language, and creativity (Figure 5). Most of the volume of the brain is made up of the cerebrum covered with the cerebral cortex, which is a thick layer of neural tissue. It is divided into four lobes, namely the frontal lobe, parietal lobe, temporal lobe and occipital lobe. Within each lobe,

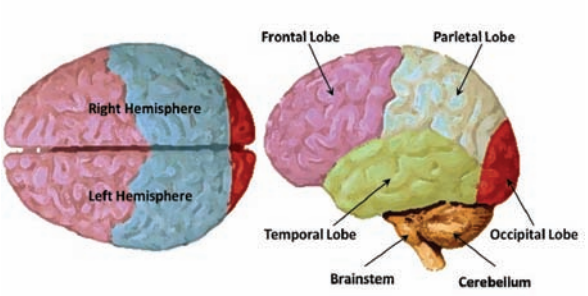

Figure 4 Anatomy of brain: Cerebral Lobes. Cerebellum and Brainstem

there are numerous areas, each associated with a particular function. The Cerebrum is separated into two hemispheres by a groove called the medial longitudinal fissure. The left and right hemispheres contain almost similar cortical areas. However, some areas show strong lateralization; especially, areas related to language are strong on the left side and areas related to spatiotemporal reasoning are strong on the right side [Kandel *et al.*, 2000]. The Cerebrum sits on top of the brainstem, which is a bundle of cranial nerves that connect the brain to motor and sensory systems in the rest of the body. It also plays an important role in the regulation of cardiac, respiratory functions, the sleep cycle and facial movements. The Cerebellum is situated behind the brainstem and below the cerebrum. It also has a cortical layer with a horizontally furrowed surface called the cerebellar cortex. This part of the brain plays an important role in motion control. Though it does not initiate the impulse for motion, it receives and integrates inputs from sensory systems and the spinal cord to fine- tune motor activities [Gray, 2008].

3.1.1 Electroencephalogram (EEG)

An Electroencephalogram can be defined as a recorded electric field of the human brain. It can be attributed to phenomena which are largely classified into three categories: spontaneous activity, evoked potentials and bioelectric events produced by single neurons. Spontaneous activity implies all the neural activities that occur continuously in the living individual and is measured on the scalp or on the brain surface. The respective components are the most prominent features of EEG signals, with amplitude of about 100μV on the scalp and 1-2 mV on the brain surface. The signal frequency bandwidth is between 1Hz and 50 Hz. Evoked potentials arise in response to a stimulus (auditory, visual, electrical etc.). The relevant EEG signal amplitudes are below the noise threshold. Hence, they are discernible only after averaging the signals in response to a train of stimuli to improve the signal to noise ratio. Single- neuron bioelectric events can be recorded by using the micro/nano electrodes implanted in the brain. It is of particular importance in monitoring the activity of neural clusters to detect the asynchronous firing of neurons, which is used as biofeedback by pace-making devices.

Bioelectromagnetism of nerve cell action potential

A nerve cell has three parts (Figure 5): a cell body *soma*, numerous short *dendrites* and a single long nerve fiber *axon*. The nerve cell body is similar to that of any other cell with a nucleus,

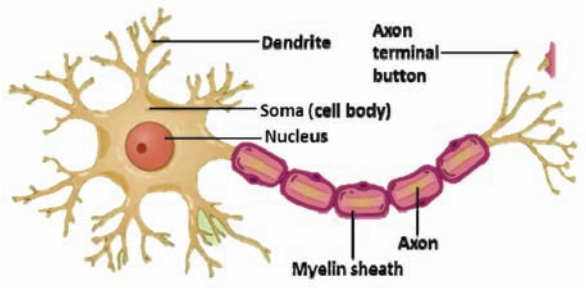

Figure 5 Nerve cell structure

mitochondria, endoplasmic reticulum and other organelles. The short dendrites receive impulses from one or more neighboring nerve cells and transfer them to the soma. The effect of these impulses can be excitatory or inhibitory. The axon fiber transfers signals from the soma to other nerve cells or muscle cells. The axon communicates with the adjacent nerve cell or muscle cell through a synapse. The neural impulse passes unidirectionally from an axonal presynaptic terminal to postsynaptic terminals on the cell through chemical neurotransmitters.

The membrane of nerve cells is a bilayer film made of ambiphillic phosphoglycerides. The cell membrane has macromolecular pores, which selectively allow sodium, potassium and chloride ions to flow through them. The difference between intra cellular ion concentration and extra cellular concentrations results in a resting trans-membrane potential V_m, where V_i is the inner surface potential and V_o is the outer surface potential of the membrane.

$$V_m = V_i - V_o \quad (1)$$

The Resting trans-membrane potential is normally negative (-70 mV). This is made possible by ionic concentration gradients of Na^+ and K^+ ions. The extracellular concentration of Na^+ is 10 times higher than intracellular concentration, whereas the intracellular concentration of K^+ is 30 times higher than the extracellular concentration (Figure 6). If a nerve cell is stimulated, can depolarize by change of in a positive direction or hyperpolarize by change of in a negative direction with respect to3. Thus, deeming the stimulus as excitatory or inhibitory, respectively [Gray, 2008].

The Excitation of a nerve cell is possible only if the stimulation impulse exceeds the threshold

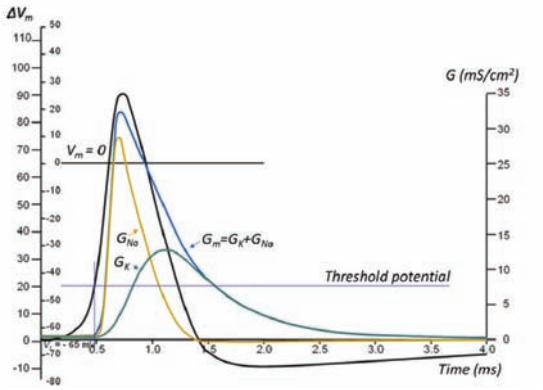

Figure 6 Action Potential: Sodium and potassium conductance (G_{Na} and G_K), their sum (G_m) and membrane voltage (V_m) during a propagating nerve impulse

potential value of 20mV, *i.e.* V_m at least, changes from -70mV to -50mV. At this point, the ionic permeability of cell membrane for a sodium ion changes very rapidly to allow a flow of sodium ions from the outside to the inside. This makes V_i more positive to the point where V_m reaches 20 mV, which is followed by a rapid change in the permeability of potassium. This allows the potassium ion to move from the inside to the outside, thus bringing V_i back to its resting value. The duration of this V_m impulse is ~1 ms. This is followed by the restoration of intra and extracellular ionic concentrations by the action of a Na-K pump, which is another macromolecular pore in the membrane [Gray, 2008].

The stimulus voltage results in a traveling action potential from one nerve to another or to a muscle cell following the path -dendrites-soma-axon-. The action potential is produced by the ion transport of Na^+, K^+ and Cl^- through the membrane. It depends mainly on the ratio of the ion concentration inside and outside the membrane, voltage across the membrane and the membrane permeability of each ionic species. Under the quasi-static assumption, the ion concentration ratio and the membrane permeability are represented by Nernst voltage at V_n temperature T (°K) in Equation (2), where R is the universal gas constant $c_{i,n}$ *and* $c_{o,n}$ are ionic concentrations of the n^{th} species, is the mole of electrons transferred during the reaction of n^{th} species and F is Faraday's constant. The driving force for the transportation, thus of n^{th} ionic species, is given by $(V_m - V_n)$.

$$V_n = -\frac{RT}{z_n F} \ln \frac{c_{i,n}}{c_{o,n}} \quad (2)$$

The EEG signal arises from the field created by localized depolarization i.e. excitatory postsynaptic potential (EPSP) or localized hyper-polarization i.e. inhibitory postsynaptic potential (IPSP). Though the stimulus potential originates at the synaptic terminals and the resultant pulse (current) travels along the neural axon fibers, electrophysiological models consider the potential source with a volumetric distribution and a conducting medium that extend continuously in three-dimensional space. They are referred to as the *volume source* and the *volume conductor*.

The Bioelectric activity of nerve cells and muscle cells due to the conversion of energy from the chemical to the electric form gives rise to a non-conservative current. This bioelectric source consists of electric current dipoles formed by charge separation. Hence, the impressed current density $\vec{J}^i(x,y,z,t)$ is similar to the volume dipole moment density of the *volume source*, where $\vec{J}^i$ is zero outside of the active cells. An infinite homogeneous conductor is a simple approximation of a *volume conductor*. The total current density can be given by Equation (3). The primary sources $\vec{J}^i$ establish electric field $\vec{E}$ and resultant return current $\sigma\vec{E}$. The return current avoids a charge buildup.

$$\vec{J} = \vec{J}^i + \sigma\vec{E} \tag{3}$$

Under quasi-static conditions, any change in the source results in a redistribution of charges across the membrane. This is expressed mathematically as follows;

$$\vec{\nabla}\cdot\vec{J}^i = \vec{\nabla}\cdot\vec{J} - \sigma\vec{\nabla}^2 V = -\sigma\vec{\nabla}^2 V \quad where\ \vec{E} = \vec{\nabla}V \tag{4}$$

This Poisson's equation in *V* can be solved to get

$$4\pi\sigma V = -\iiint_{Vol}\left(\frac{1}{r}\right)\vec{\nabla}\cdot\vec{J}^i dVol \tag{5}$$

This solution can be extended to an inhomogeneous volume conductor, considered as composed of a finite number of homogeneous regions. The head as a volume conductor consists of the brain, cerebrospinal fluid, skull and scalp, not to mention that the brain tissue can be divided into gray matter, white matter and other tissue. Each p^{th} homogeneous region (uniform conductivity σ and unit volume dv_p) has a boundary S_p, which satisfies the conditions of the continuity of electric potential *V* (6) and the normal component of current density (7). Subscripts 1 and 2 represent either side of boundary S_p.

$$V_1(S_p) = V_2(S_p) \tag{6}$$

$$\sigma_1\vec{\nabla}\left(V_1(S_p)\right)\cdot\vec{n}_p = \sigma_2\vec{\nabla}\left(V_2(S_p)\right)\cdot\vec{n}_p \tag{7}$$

Following the same steps as shown in Equations (3), (4) and (5) [Geselowitz, 1964], the new expression for *V* is

$$4\pi\sigma V = -\iiint_{Vol}\left(\frac{1}{r}\right)\vec{\nabla}\cdot\vec{J}^i dVol + \sum_p\iint_{S_p}(\sigma_{p,2}-\sigma_{p,1})V\vec{n}_p\cdot\vec{\nabla}\left(\frac{1}{r}\right)d\vec{S}_p \tag{8}$$

The first term on the right hand side is the contribution of the volume source because of the non-electric energy source $\vec{J}^i$. The second term contribution of a surface source is the summation dipole elements that represent ionic double layers, described by Equations (6) and (7). Since neural tissue is composed of a very large number of small nerve cells, can be summed up as a volume dipole moment density function.

$$\vec{J}_i = \frac{\sum_{p=1}^{N} d\vec{\eta}_p}{\sum_{p=1}^{N} dv_p} \quad where\ d\vec{\eta}_p = \int(\sigma_o V_o - \sigma_i V_i)d\vec{S}_p \tag{9}$$

In an electrophysiological measurement, *V* can be measured. Thus, Equation (8) describes a problem where the field and the volume conductor are known, but the volume source is unknown. Such problems are called Inverse Problems [Malmivuo *et al.*, 1995]. This pertains to clinically measured EEG, where the neurologists seek to determine the source of the measured bioelectric signal (EEG). A Similar principle obtains with other electrophysiological signals such as ECG, EOG and EMG. Though it is possible to evaluate the source function $\vec{J}^i$ in the case of ECG and EMG, it has not been completely feasible in EEG because of

the complexity of the brain structure and its electrophysiological behavior. Quantitative EEG is largely based on an examination of lead patterns to calculate the sensitivity distribution of lead and estimate the statistically most probable source configuration i.e. neurological conditions. However, clinical EEG diagnostics is typically based on the recognition of typical signal patterns that are known to be associated with neurological conditions [Fine *et al.,* 2002].

3.2 Cardiovascular Anatomy and Electrophysiology

The human heart is a muscular organ consisting of four chambers: two upper chambers known as the *atria* and two lower chambers known as the *ventricles*, which are separated by a muscular septum into the right and left atria and ventricles respectively (Figure 7(a)). Oxygen depleted blood from the peripheral organs are returned to the right atrium through the Superior and inferior venacava. The contraction of the right atrium then forces blood into the right ventricle through a unidirectional heart valve known as the *tricuspid valve.* The Right ventricle then contracts and pumps blood into the pulmonary artery which takes the blood to the right and left lungs to exchange the carbon dioxide in the blood for fresh oxygen. Meanwhile, freshly oxygenated blood from the lungs is brought to the left atrium by the pulmonary vein. The left atrium then contracts and forces the blood into the left ventricle through a unidirectional valve called the *mitral* or *bicuspid valve*. The Contraction of the left ventricle forces the blood through the semilunar valve into the aorta which then branches out to several arteries and supplies fresh blood to all the cells in the body. The major blood vessels involved in the supply of blood to the cardiac tissue are the Left and Right Coronary arteries that branch off from the aorta as shown in Figure 7 (b).

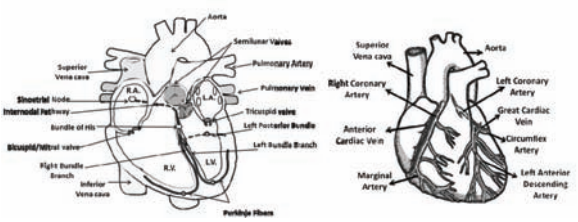

Figure 7 (a) A diagram of the internal anatomy of the heart with the impulse conduction pathway (b) Illustrates the blood vessels involved in the circulation of blood to the heart muscles.

3.2.1 Origin of Cardiac Electrophysiology – Cardiac Action Potential

Cardiac muscle cells or *myocytes* have a resting potential varying between -80mV and -90mV. The resting (transmembrane) potential (TP) difference is between the intracellular fluid and the extracellular fluid. This potential difference is maintained by the selectively permeable cell membrane that in turn, maintains the difference in the sodium, potassium, calcium, chloride and potassium ion concentrations between the two fluids. The TP is regulated predominantly by Sodium and Potassium ion concentrations. The cell membrane has voltage-activated channels that transport ions into or out of the cell when triggered by a voltage impulse. As the voltage- gated channels on the cell membrane are activated or deactivated by a voltage impulse travelling across the cell, the transmembrane potential varies with time. Figure 8 illustrates the time variation of the transmembrane potential in a single cardiac myocyte upon the arrival of an impulse.

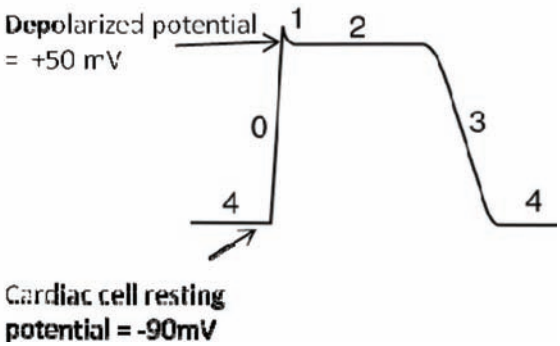

Figure 8 Transmembrane potential variations over time for a single cardiac myocyte.

The transmembrane potential variation during the conduction of an impulse is called action potential. Upon the arrival of a positive impulse that shifts the TP above -70mV, a *threshold voltage*, rapid depolarization and the movement of TP towards positive potentials occurs. This is due to the opening of the Sodium gated channels and the rapid influx of sodium ions. Following this, potassium and chloride ion channels open and cause the TP to drop a little towards 0mV. This dip is denoted as Phase 1. In Phase 2, the influx of sodium ions, along with some Calcium ions and the efflux of Potassium ions are in equilibrium and the TP is maintained at a constant value. Phase 3 is the repolarization step when TP moves towards the resting TP. In this

phase, the Potassium ions are rapidly exchanged for sodium ions inside the cells to restore the initial ionic balance at the resting TP. The Calcium ion channels also reduce their conductance during this phase. Phase 4 is the resting TP condition. The cell processes from Phase 0 result in an increased intracellular Calcium ion concentration in the muscle tissue which initiates the release of energy by the breaking down of adenosine triphosphate (ATP) molecules and conformational changes in proteins that result in muscle contraction. The coupling between the Ca ion and its role in muscle contraction are discussed in greater detail elsewhere [Reisner, 2007].

3.2.2 Cardiac Impulse Conduction Physiology

The heart has a small group of cells called sinuatrial nodes located in the right atrium that are capable of generating impulses periodically. These impulses maintain the contraction rhythm of the heart and their direction of propagation maintains the progression of contraction i.e. the atria contract first, then the ventricles. It is often referred to as the natural pacemaker of the heart as it directly regulates the heart rate. Impulses are fed to the sinuatrial node by the *Vagus nerve* and *parasympathetic and sympathetic nervous systems*.

At the beginning of the cardiac cycle, the sinuatrial node generates an impulse which is carried to the *atrioventricular node* or the *Bundle of His* through the internodal pathway, which is made of a fiber of specially modified muscle cells. The atria contract as the impulse is conducted through the internodal pathway. From the atrioventricular node, the conduction pathways split into the left bundle branch and the right bundle branch. The left bundle branch conducts the cardiac impulse along the left ventricle, while the right bundle branch conducts the impulse along the left ventricle. Both bundle branches end in Purkinje fiber cells which are tree shaped and spread the cardiac impulse along the entire surface of the ventricles. Figure 7(a) illustrates the electrical conduction pathway from the sinuatrial node to the Purkinje fibers.

3.2.3 Electrocardiograph (ECG) and Bioelectromagnetic origin and Dipole Theory for ECG

The electrocardiogram (ECG) is a simple non-invasive test to observe the variations in biopotentials originating from the heart, through electrode sensors placed on the surface of the skin. The ECG waveform acquired from a derived Lead II electrode placement system is shown in Figure 9, which clearly depicts the classical components of the ECG waveform. The waveform characteristics of the ECG include the P wave, QRS complex, T and U waves.

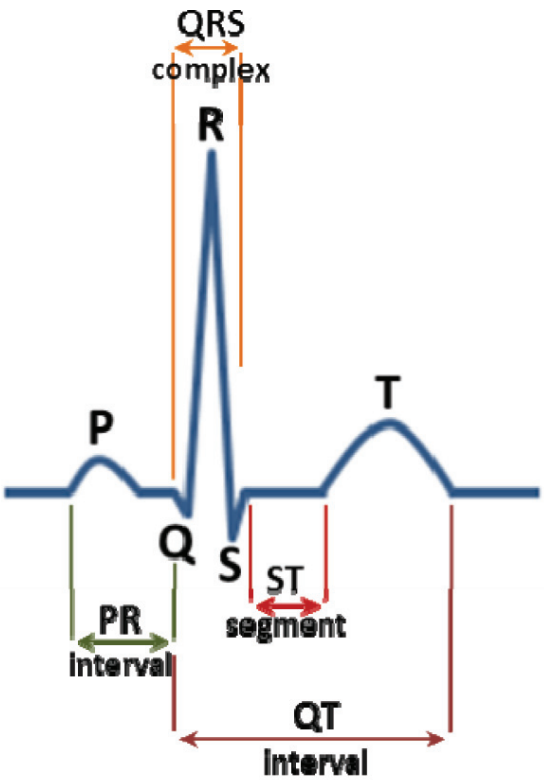

Figure 9 ECG waveform with the characteristic P wave, QRS complex, T and U waves.

The P wave represents the wave of depolarization that spreads from the Sino-Atrial node throughout the atria, and is usually 0.08 to 0.1 seconds in duration. The QRS complex represents ventricular depolarization. The isoelectric period following the QRS complex is the time at which the entire ventricle is depolarized and roughly corresponds to the plateau phase of the ventricular action potential. The T wave represents ventricular repolarization and is longer in duration than depolarization. It is followed by a U wave whose origin is not well understood. There are three popular hypotheses: (a) late repolarization of Purkinje fibers, (b) late repolarization in the left ventricle, and (c) after-potentials causing variations in normal

potentials. In normal subjects, U waves have the same polarity as T waves.

The Dipole Theory for ECG

The ECG is electrical activity observed at the surface of the skin. The most widely followed theory that bridges the origin of cardiac activity and the ECG is the dipole theory [Geselowitz, 1964]. The derivations presented in this chapter are based on the material in [Reisner, 2007].

The development of this theory can be divided into three fundamental steps:

1. A model for Cell membrane conduction of action potential– **Cable Model.**
2. A Representation for the electrical activity propagated from one cell to its neighbor – **Dipole Cardiac Vector.**
3. A model for the transduction of this electrical activity from the heart to the surface of the torso – **Derivation of ECG from the Dipole vector.**

Cable Model

The cable model is used to describe the transmembrane potential variations and the currents flowing both inside and outside the myocardial cell. Figure 10 illustrates the electrical circuit equivalent of the cell membrane.

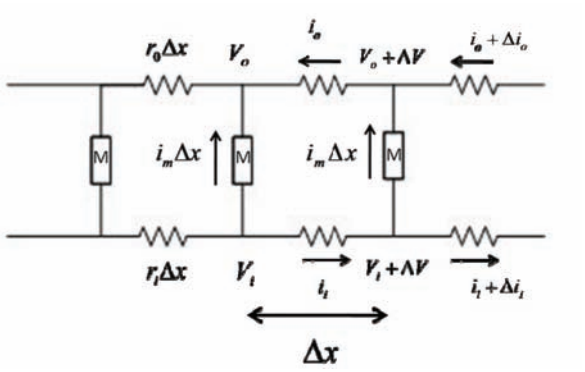

Figure 10 The circuit model for currents and voltages at the cell membrane.

V_o and i_o are the extracellular voltage and current at a given instance. V_i and i_i are the intracellular voltage and current at a given instance. M represents the lumped properties over a length $\Delta\chi$. r_o and r_i are the resistances per unit length, of the extracellular and intracellular fluids, respectively. i_m is the current flowing through the membrane per unit length. The TP is given by $V_m = V_i - V_o$ along the membrane. Based on this model, we can arrive at a relationship between the rate of change of TP with respect to position and the ionic current.

$$i_i r_i \Delta x = -\Delta V_i \tag{10}$$

$$\frac{\partial V_i}{\partial x} = -i_i r_i \tag{11}$$

Similarly,

$$\frac{\partial V_o}{\partial x} = -i_o r_o \tag{12}$$

Using Kirchoff's current law at one of the nodes,

$$\Delta i_i = -i_m \Delta x \tag{13}$$

$$\frac{\partial i_i}{\partial x} = -i_m \tag{14}$$

$$\frac{\partial V_m}{\partial x} = \frac{\partial (V_i - V_o)}{\partial x} = \frac{\partial V_i}{\partial x} - \frac{\partial V_o}{\partial x} = -i_i(r_i + r_o) \tag{15}$$

The TP varies with time as well as spatially.

$$i(x,t) = -\frac{1}{(r_i + r_o)} \frac{\partial V_m(x,t)}{\partial x} \tag{16}$$

Substituting for membrane current from (14)

$$i_m(x,t) = \frac{1}{(r_i + r_o)} \frac{\partial^2 V_m(x,t)}{\partial x^2} \tag{17}$$

Dipole Cardiac Vector

At the interface between a depolarized myocardial cell and the neighboring resting cell, there is a transmembrane current that follows to negate the difference in the TP between them. This ionic current flow can be depicted as shown in Figure 11.

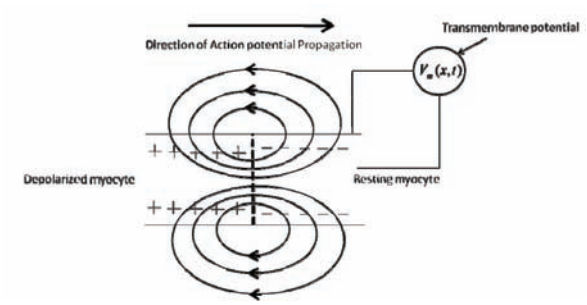

Figure 11 Propagation of transmembrane current at the interface between a resting myocyte and a depolarized myocyte.

On the assumption that the travelling action potential has a constant velocity (c) and shape within the myocardium we have,

$$\frac{\partial V_m(x,t)}{\partial x} = \frac{\partial V_m(x,t)}{\partial t} \cdot \frac{\partial t}{\partial x} = \frac{1}{c} \cdot \frac{\partial V_m(x,t)}{\partial t} \tag{18}$$

$$i = -\frac{1}{(r_o + r_i)} \cdot \frac{1}{c} \cdot \frac{\partial Vm(x,t)}{\partial t} \tag{19}$$

This current flowing between a depolarized and a resting myocyte forms a current dipole. The vector associated with this dipole is the dipole moment as shown below in Figure 12 by the hypothetical, spherical interface between a depolarized and a resting myocyte.

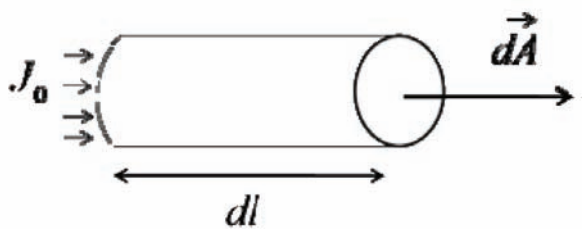

Figure 12 Unit dipole produced by the current flowing through a hypothetical spherical interface between a depolarized and a resting myocyte.

The magnitude of the dipole moment is given by,

$$\vec{m_o} = j_0 . \vec{dA} . dl \quad (20)$$

Where $\vec{m_o}$ is the unit dipole moment vector, $\vec{dA}$ represents the direction of the dipole moment and unit increment in a cross sectional area of the cardiac myocyte. *dl* is the length of a unit dipole vector. and are several orders of magnitude smaller than the length spanned by the electrodes on the torso. Therefore, it is acceptable to represent them as infinitesimal increments.

The Values for $\frac{\partial V_m(x,t)}{\partial t}$, r_i, r_o, r_i, r_o and *dl* can be estimated and verified experimentally, yielding a quantitative value for the dipole moment vector.

The heart as a source of the potential, however, is the resultant summation of all individual dipole moments originating from the cardiac myocyte. Given by,

$$M_0 = \iiint J . \vec{dA} . dl \quad (21)$$

Derivation of ECG from Dipole Vector

According to the dipole theory, the potential difference measured across two points on the torso is the geometric projection of the cardiac vector on the line vector connecting the two points. The aim therefore, is to derive the relationship between the Cardiac Dipole vector and the surface potentials at the level of the skin. For the sake of simplicity, the relation between the dipole vector and surface potential at the skin is derived for a single instant of time. By expressing the dipole moment as a function of time, a real time expression for ECG can be derived with ease.

The following assumptions are made in the derivation

1. The torso is a linear, isotropic, homogeneous, spherical conductor of radius *R* and conductivityσ.
2. The heart's activity is represented by the time varying Cardiac Dipole vector.

Within the spherical torso, linearity dictates,

$$\vec{J} = \sigma \vec{E} = -\sigma \nabla \varphi \quad (22)$$

Where $\vec{E}$ is the electric field and Φ is the electric potential. Since the net charge generation through the cardiac cycle is 0,

$$\nabla \vec{J} = 0 \quad (23)$$

From (26),

$$\nabla^2 \varphi = 0 \quad (24)$$

This is a Laplacian equation which is solved in spherical coordinates with the following boundary conditions,

1. No current is allowed to flow out of the body. Therefore, $\frac{\partial \varphi(r,\theta)}{\partial r} = 0$ at r = R (radius of torso)
2. Condition established in the dipole cardiac vector derivation. $M_0 = \iiint J . \vec{dA} . dl$

The solution that satisfies the boundary conditions is written as a sum of two functions

$$\varphi(r,\theta) = \varphi_1(r,\theta) + \varphi_2(r,\theta) \quad (25)$$

$$\varphi(r,\theta) = \frac{M_0}{4\pi\sigma} cos\theta \left[\frac{1}{r^2} + \frac{2r}{R^3}\right] \quad (26)$$

At the surface of the sphere i.e. the skin on the torso, r = R

$$\varphi(r,\theta) = \frac{3M_0}{4\pi\sigma R^2} cos\theta \quad (27)$$

The Figure 13 (a) and (b) illustrate how the potential at the surface is calculated as a projection of the cardiac dipole vector.

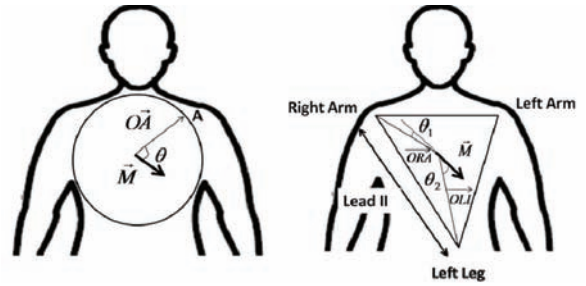

Figure 13 (a) Relation between the cardiac dipole vector and the potential at a point on the surface of the skin (b) Ideal Torso

The vector representation of (27) is,

$$\varphi_A = \vec{M} \cdot \overrightarrow{OA} \tag{28}$$

Substituting for $\vec{M}$ from (21) and j_0 from (17),

$$\varphi_A = \iiint \left[\frac{1}{r_o+r_i} \cdot \frac{1}{A_{cr}} \frac{\partial^2 V_m(x,t)}{\partial x^2} \cdot \overrightarrow{dA}.dl\right] \cdot \overrightarrow{OA} \tag{29}$$

Lead II refers to the measurement of the potential difference between the electrodes placed on the right arm and the left leg. Based on this result, the ECG for the lead II position is calculated as follows,

$$V_{II} = \varphi_{LL} - \varphi_{RA} \tag{30}$$

$$\varphi_{LL} = \vec{M}.\overrightarrow{OLL} \tag{31}$$

$$\varphi_{RA} = \vec{M}.\overrightarrow{ORA} \tag{32}$$

$$V_{II} = \vec{M}.(\overrightarrow{OLL} - \overrightarrow{ORA}) \tag{33}$$

3.3 Monitoring and Diagnosis: Neurological Signal Measurements of Diagnostic value

Electroencephalogram (EEG) measurement

EEG is the recording of the electrical activity of the brain along the scalp region by measuring the fluctuation in the voltage induced by the ionic current flows that originate from the neurons. EEG is normally measured by placing the electrodes over the skull at defined positions according to the international 10-20 system (Figure 14) [Niedermeyer *et al.*, 2004]. The 10 and 20 refer to the distance

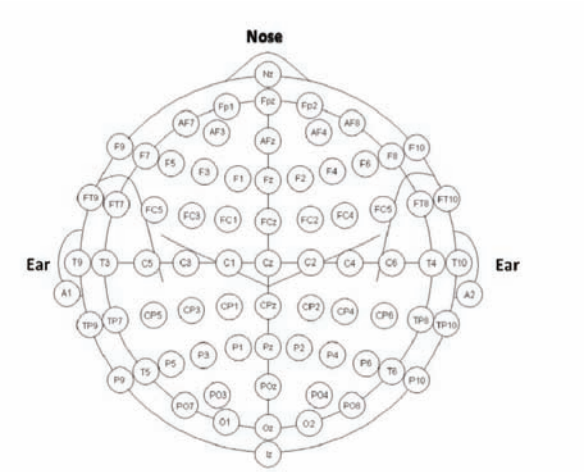

Figure 14 International 10-20 placement of electrodes for EEG

between adjacent electrodes by dividing the transverse and median planes of the skull perimeters into 10% and 20% intervals. In the international 10-20 system, 19 electrodes are placed over the skull and 2 electrodes are placed on the ears as reference electrodes. The letters F, O, C, P, T in the 10-20 system of placement of electrodes stand for Frontal, Occipital, Central, Parietal and Temporal respectively. The electrodes are placed according to the location of placement and the underlying cerebral cortex. The even numbers represent the right side of the hemisphere and the odd numbers represent the left side of the hemisphere. There are two basic methods by which the electrodes are placed: monopolar and bipolar. In monopolar, one side of the amplifier is connected to the reference electrode and in bipolar, the amplifier is connected between a pair of electrodes. The electrical activity is acquired and amplified/filtered to record EEG waveform Table 1.

Electrooculogram (EOG) measurement

An Electrooculogram is the measurement of the resting potential of the retina. EOG monitors the eye movements by detecting the dipolar current flowing from the cornea to the retina, which also indicates the angular displacement of the eye. The Applications of EOG include saccadic movements, smooth pursuit movements, convergence/ divergence to record and optokinetic nystagmus. Normally, the electrodes are placed around the eyes with a reference electrode on the forehead. The electrodes are placed on the temple for the lateral movement and the other electrodes are placed vertically, one above and the other below the eye

Table 1: EEG and its characteristics

Electrical Activity	Frequency of occurrence	Characteristics
Beta Activity	13-30 Hz Frontal and parietal lobe	Normal activity present when the eyes are open or closed. Some drugs increase the amount of beta activity in the EEG
Alpha Activity	8-13 Hz Occipital lobe	Also a normal activity when present in waking adults. It is only seen when the eyes are closed and should disappear or reduce in amplitude when the eyes are open
Theta Activity	4-8 Hz Back and Central areas of the brain	It can be classed as both a normal and abnormal activity depending on the age and state of the patient. In adults it is normal if the patient is drowsy. However it can also indicate brain dysfunction if it is seen in a patient who is alert and awake.
Delta Activity	0.5-4 Hz	It is only normal in an adult patient if they are in a moderate to deep sleep. If it is seen at any other time. It would indicate brain dysfunction. Abnormal activity may be seen in all or some channels depending on the underlying brain problem. It can be shown to the depressed person
Spike and Wave Activity	Random frequency < 60 Hz	Number of other waveforms, which are more specific to certain conditions. For example spike and wave activity indicates a seizure disorder. Other epileptic conditions may be diagnosed if spikes or sharp waves are seen

(Figure 15) to measure the vertical movement of the eyes [Niedermeyer *et al.*, 2004].

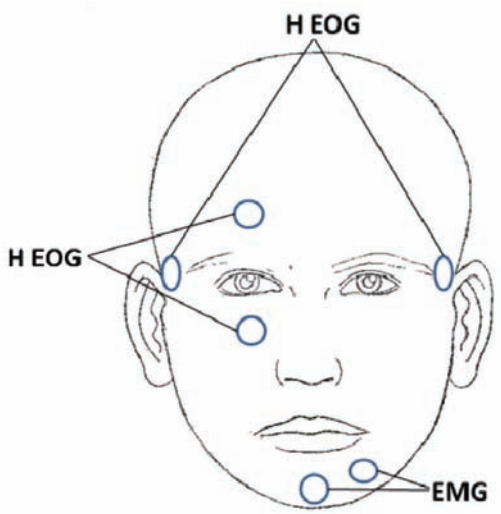

Figure 15 Standard electrode placements for EOG for monitoring vertical (V) and horizontal (H) eye movement and EMG for reliable detection of muscle tone REM sleep

Electromyography (EMG) measurement

EMG depends on the firing action potential of the numerous motors present in the muscles. The electrodes placed on the skin over the muscle detect the electrical activity of the muscles of the underlying tissues (Figure 15). It is difficult to correlate the waveform with the specific muscle from which it is generated, but this difficulty can be alleviated by the proper placement of the electrodes. The muscle fibers which are present near the electrodes will have a greater impact on the waveforms, whereas the muscles at a distance will have less impact with respect to signal strength. This dependence of the quality of EMG on the distance of the muscles and electrodes is mainly caused due to the impedance between the tissues. Therefore, placing the electrodes at a distance will provide varying and more generalized signals, and placing the electrodes at short intervals gives a signal which is more specific to the muscles over which the electrodes are placed. However, it becomes nearly impossible

to identify the specific muscles generating the signal because of the interference from noise and motion artifacts. The electrodes are generally placed in parallel with the dominant muscles, since this minimizes signal cancellation and maximizes biofeedback sensitivity [Wolpaw *et al.*, 2002].

Neurological Signal Abnormalities

Symptoms ranging from structural, biochemical or electrical abnormalities in the nervous system, especially the brain and the nerves, which denote abnormality, are termed a neurological disorder. The two fields of medicine, neurology and neuropsychology, deal with most types of neurological disorders. These disorders may vary from loss of concentration to paralysis, where they are also classified into common and rare categories depending on the degree of impact [Levi-Montalcini, 2007]. They are one of the 10 leading causes of deaths in the United States of America. They are followed by infectious diseases such as meningitis and tetanus. Equally prevalent are degenerative neurological disorders such as Alzheimer's disease and Parkinson's disease [CDC, 2013]. A range of specific disorders can be identified and diagnosed with biopotential signals such as electroence phalography (EEG), electrooculography (EOG) and electromyography (EMG), (Table 2).

Table 2: Biopotential and Neurological disorders

EEG	• Tumors • Stroke • Epileptic seizures • Encephalopathy or delirium • Catatonia • Alzheimer's • Parkinson's
EOG	• Clinical ophthalmology • Parkinson's • Sleep disorders
EMG	• Axillary nerve dysfunction • Centronuclear myopathy • Mononeuritis multiplex • Motor neuron disease • Neuromyotonia • Peripheral neuropathy

3.4 Monitoring and Diagnosis: Cardiological Signal Measurements of Diagnostic value

Electrocardiography (ECG) Measurement

The Electrocardiogram (ECG) is a fundamental non-invasive method for monitoring the heart's electrical activity by placing electrodes on the skin. The ECG provides multiple perspectives of the heart's electrical activity simultaneously [Garcia *et al.*, 2001]. The setup can be a 3 lead system with electrodes placed at the corners of the torso section of the body (Figure 16) as a substitute to the extremities of the limbs (right arm, left arm and left leg), thus forming an imaginary triangle known as Einthoven's Triangle. They provide a limited view of electrical cardiac activity, but the polarity of these leads is useful for determining the direction of propagation of the depolarizing pulse through the cardiac tissue known as the electrical axis. The setup can also be a 12 lead system (Figure 16), which uses 10 electrodes, 4 placed at the extremities of the limbs (arms and legs) and 6 placed on the chest. The 6 chest electrodes are called precordial leads that give a perspective of electrical cardiac activity in a horizontal plane that is orthogonal to the electrical axis [Brosche, 2010]. For chronic disease management, out of hospital rehabilitation and diagnostics such as event detection require a full time ECG recording on ambulatory patients. For this, the 12 lead ECG setup can be simplified to a 5 electrode system known as the EASI system and simple mathematical transformations exist to derive the 12 lead ECG. These 5 electrodes are on the upper part of the body along the sternum and midaxial region [Jahrsdeorfer *et al.*, 2005; Khan, 2007]. Hence, the ECG panel can be used as an image of the cardiac activity for non-invasive medical diagnosis.

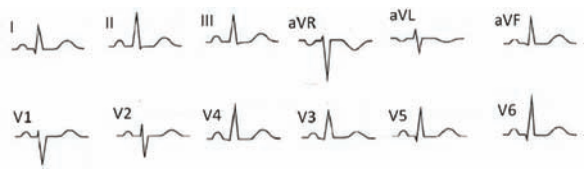

Figure 16 Electrode placements for 3-lead and 12-lead ECG, signals from 12 Leads [77,79].

Electrical Impedance Tomography (EIT)

Trans Thoracic Impedance (TTI) is a technique used to measure the change in impedance across the thoracic cavity. It is a type of Electrical Impedance Tomography (ETI) technique. It is important for monitoring pulmonary function, trans-myocardial current, cardiac output and the overall fluid retention of the thoracic cavity. The latter is important in the monitoring of hypertensive patients.

The set up uses 4 electrodes placed in the sub-clavicle, sub-axillar, anterior or posterior positions (Figure 17). A constant current is applied to 2 electrodes and the resulting voltage is recorded across the other 2 electrodes. The electrode pairs are placed across the thoracic cavity from each other to capture a change in conductivity due to the ventilation of the lungs or cardiac function. This system is also capable of acquiring an impedance image of the thoracic region by using an electrode array (16 electrodes or more) placed all around the thoracic cavity. Each set of 4 electrodes acts as a perspective (angle) for scanning the bioimpedance.

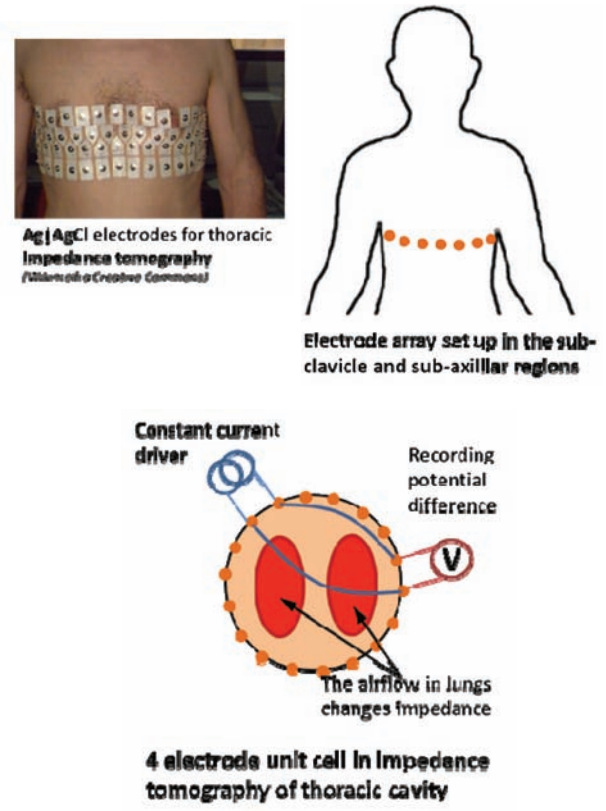

Figure 17 Electrical Impedance Tomography (EIT) of thoracic cavity to lung function

The 4 electrode system includes the electrodes, a current driver (source), a voltage recording unit and a phase-sensitive demodulator. The phase demodulator records voltage values while in phase with the current source and at a phase delay of 90° to extract the resistance and reactance values of the bioimpedance. The Applied current is $1/10^{th}$ of the current threshold for causing any sensation on the skin. The Input current frequency is kept around 50 kHz. At this frequency, the impedance characteristics of the tissue are similar to those at D.C. That is, the current travels in extracellular space but the electrode-skin impedance is much lower than that at D.C. Hence, there is less instrumentation error due to baseline noise and impedance mismatch. However, measurements taken across a frequency spectrum can help in rectifying any phase effects [Holder, 2005].

Early systems such as the Sheffield Mark 1 used a single impedance measurement circuit and a multiplexer to link with the array of electrodes. More recent systems use devoted circuits for each electrode set. While the former is portable but slow, the latter is fast but bulky. Two types of electrodes are commonly used for this system, silver-silver chloride gel electrodes and the conductive gel filled gold cup electrode.

In theory, the EIT system should be free of impedance at the electrode-skin interface. In practice, skin preparation (abrasion) is used for reducing impedance at the electrode-skin interface. Still, the system experiences a change in impedance at the interface. During thoracic impedance monitoring for longer periods of time, the conductive gel may dry up and increase electrode-skin impedance. Dry textile based nano-biosensor electrodes have a contact impedance less than that of the plain dry electrodes; hence, they can be a good alternative to gel- based electrodes for long term monitoring.

Cardiological Signal Abnormalities

Cardiovascular disorders can be diagnosed by identifying ECG abnormalities and computing their frequency of occurrence. This is accomplished by the following diagnostic criteria that are mentioned in Table 3.

Apart from the well-defined diagnostic criteria mentioned above, there are a few approaches that are being researched to eventually be included in standard clinical practice. Ventricular Arrhythmias are abnormalities in the cardiac conduction physiology or anatomy originating in the Ventricles of the heart. From a cardiac patient care perspective, they are a cause of immediate concern because they can lead to fatal outcomes like Sudden Cardiac Arrest (SCA) leading to Sudden Cardiac Death (SCD) and Acute Myocardial Infarction (AMI).

Table 3: Diagnostic criteria for cardiovascular disorders based on ECG abnormalities [Wu.V.C et al, 2005]

ECG wave characteristic	Abnormal Morphology	Additional Criteria	Lead of interest	Diagnosis
P Wave	Inverted	II, III and aVF but upright in aVR	II, III, aVF and aVR	Atrioventricular Junctional or ectopic atrial rhythm.
	Absent		All leads	Sinoatrial Block and Atrioventricular junctional rhythms.
	Wave duration e > 0.12 seconds		II, III and aVF	Left atrial enlargement
	Elevated P wave amplitude	Positive amplitude > 0.25mV	II, III or aVF	Right atrial enlargement. Also consider right ventricular hypertrophy, cor pulmonale, pulmonary hypertension, pulmonary and bicuspid stenosis.
		Amplitude of first half of V1 or V2 > 0.15mV	V1, V2	Right atrial enlargement.
	Notched (has 2 peaks)	Distance between peaks of > 0.04 seconds	II, III and aVF	Left atrial enlargement
	Biphasic	negative amplitude < 0.1mV and duration <0.04 seconds	V1	Left atrial enlargement
		Positive amplitude > 0.15mV and negative amplitude > 0.1mV	V1	Biatrial Enlargement
ST segment	Elevation	Elevation > 0.1m V and chest pain	2 or more contiguous leads	ST elevation Myocardial Infarction (STEMI)
		Marked ST elevation in Leads II, III and aVF accompanied by marked reciprocal depression in Leads I and aVL	I, II, III, aVL and aVF	Acute inferior Myocardial Infarction (MI) V1- V5 Extensive acute anterior MI
		Marked ST Elevation in V1-V5		
	Depression	ST depression > 0.1mV and Creatinine Kinase MB test positive	2 or more contiguous leads	Non-ST elevation MI
		ST depression >0.1mV and Creatinine Kinase MB test negative	2 or more contiguous leads	Ischemia

Q wave	Duration > 0.0 4 seconds, Amplitude >0.3mV	Lead III and a VL amplitude > 0.7mV, Lead I amplitude > 0.15mV	II, III and aVF	Inferior MI, possible - hypertrophic Cardiomyopathy, Wolff-Parkinson-White Syndrome
			V1- V4	Anterior MI
			V5-V6	Lateral MI, Hypertrophic Cardiomyopathy.
			I, aVL, V5, V6	Anterolateral MI
R wave	Voltage amplitude criteria	< 0mV or > 0.6mV on V1, d" 0.02mV in V2, < 0.1mV in V3	V1-V6	Anterior MI, Left Ventricular Hypertrophy, Left Bundle Branch Block if QRS duration >0.12 seconds, Emphysema
T wave	Peaked		V1 - V6	Hyperkalemia
			V1 and V2	Posterior MI
	Inversion with abnormal Q waves or > 0.1mV ST elevation or depression	Inversion in Lead I, II and V3 to V6, upright in a VR	I,II,aVR, V3 - V6	Ischemia
	Inversion with normal ST segment	Deep Inversion > 0.5mV	V2 - V5	Ischemia or Posterior MI
			II, III, aVF and aVR	Ischemia or Posterior MI
			Several Leads	Cardiomyopathy
		Minor inversion < 0.5mV		Non-specific - maybe Ischemia, Electrolyte depletion, Alcohol abuse, cardiomyopathy, Myocarditis or others
QRS complex	QRS duration > 0.12 seconds.	A secondary R wave in V1 or V2, Slurred S wave in V5, V6 and Lead I with duration > 40ms. S wave is longer in duration than the preceding R wave in Leads V6 and I	I, V1, V2, V5, V6	Right Bundle Branch Block (RBBB)
		Broad Monophasic R wave notched or slurred in Lead I, aVL, V5 or V6, Late intrinsicoid deflection in Leads I, V5, V6 greater than 0.05 seconds.	I, aVL, V5, V6	Left Bundle Branch Block (LBBB)
	Low Amplitude	< 0.5mV in Leads I,II, III, aVF,	All Leads	Obesity, Pericardial Effusion, Constrictive

		aVR, aVL or <1mV in V1- V6		pericarditis, Myxedema, Amyloidosis, pleural effusion, Chronic Obstructive Pulmonary Disease
PR Interval	Duration > 0.2 seconds		II, V1	First degree atrioventricular block,
	Duration < 0.11 seconds		II, V1	Wolff-Parkinson-White Syndrome, Atrioventricular Junctional Rhythm, Lown-Ganong-Levine syndrome.

The T wave, QT interval and the ST segment of the ECG are known to be indicative of the repolarization of the ventricles of the heart during a cardiac cycle. Consequently, among ECG analysis criteria, T wave alternans (TWA) and T wave inversion (TWI) have gained significant research interest as means to predict the likelihood of Ventricular Arrhythmias.

T-wave Alternans (TWA) - T wave alternans is the beat-to-beat variation of T wave morphology and amplitude. Several clinical studies have tried to determine the significance of using TWA analysis to detect abnormalities that may lead to Ventricular Arrhythmias, as well as to establish metrics to perform risk stratification for cardiovascular patients with prior cardiac episodes. The statistical significance of TWA in predicting ventricular arrhythmias has been established in patients across several diagnoses [Gehi *et al.,* 2005]. Studies have also shown the significance of the predictive value of TWA analysis in post myocardial infarction patients [Maeda *et al.*, 2009], risk of SCD [Merchant *et al.,* 2012], congestive heart failure [Klingenheben, 2000], ischemic cardiomyopathy [Chow *et al.,* 2006] and Chagas disease [Ribeiro *et al.,* 2011]. Figure 18 shows an example of a TWA analysis performed in [Cox *et al.,* 2007]

T-wave Inversion (TWI) - TWI is the reversal in polarity of the normal T wave which is upright in most ECG leads. TWI has been associated with cardiovascular as well as cerebrovascular abnormalities [Catanzaro *et al.,* 2008]. TWI coupled with QT interval changes and dialysate Calcium concentrations have also been associated with an increased risk of SCD among patients who have recently undergone Hemodialysis [Catanzaro *et al.,* 2008; Herzog *et al.,* 2008; Pum *et al.,* 2013; Wu *et al.,* 2005]. Moreover, TWI has gained significant research interest because of its high incidence in young athletes [Wilson *et al.,* 2012] and soldiers [Eckart *et al.,* 2004]. TWI is a known diagnostic criterion for Hypertrophic Cardiomyopathy (HCM). HCM is known to significantly increase a patient's susceptibility to a SCA leading to SCD when the patient is exposed to exertion through cardiovascular exercises. Consequently, T wave characteristics are an important criterion used in prescreening for athletes in sports and soldiers in military recruitment. As an example, Figure 19 shows the asymptomatic TWI in a Football referee [Wilson *et al.,* 2012].

QT interval dispersion: Sudden cardiac death and fatal arrhythmia are the major causes of death among dialysis patients. According to the United States Renal Data System (USRDS) database, the mortality rate among dialysis patients (hemodialysis or peritoneal dialysis) is 230 per 1000. SCD and arrhythmias account for 25% of these deaths [Herzog *et al.,* 2008]. Dialysis patients who have pre-existing heart condition(s) are at an increased risk of sudden death due to disturbances in electrolyte metabolism. QT dispersion is defined as the difference between the longest and shortest QT intervals extracted from ECG signals from single lead or multiple leads up to the complete set of 12 leads. A heart rate corrected QT interval is given by Bazett's formula $QT_c = \left(QT_{\max} - QT_{\min}\right) / \sqrt{RR_{\text{int}erval}}$. QT dispersion reflects the differences in the heart dipole vector (previous section) projects and abnormalities of T-

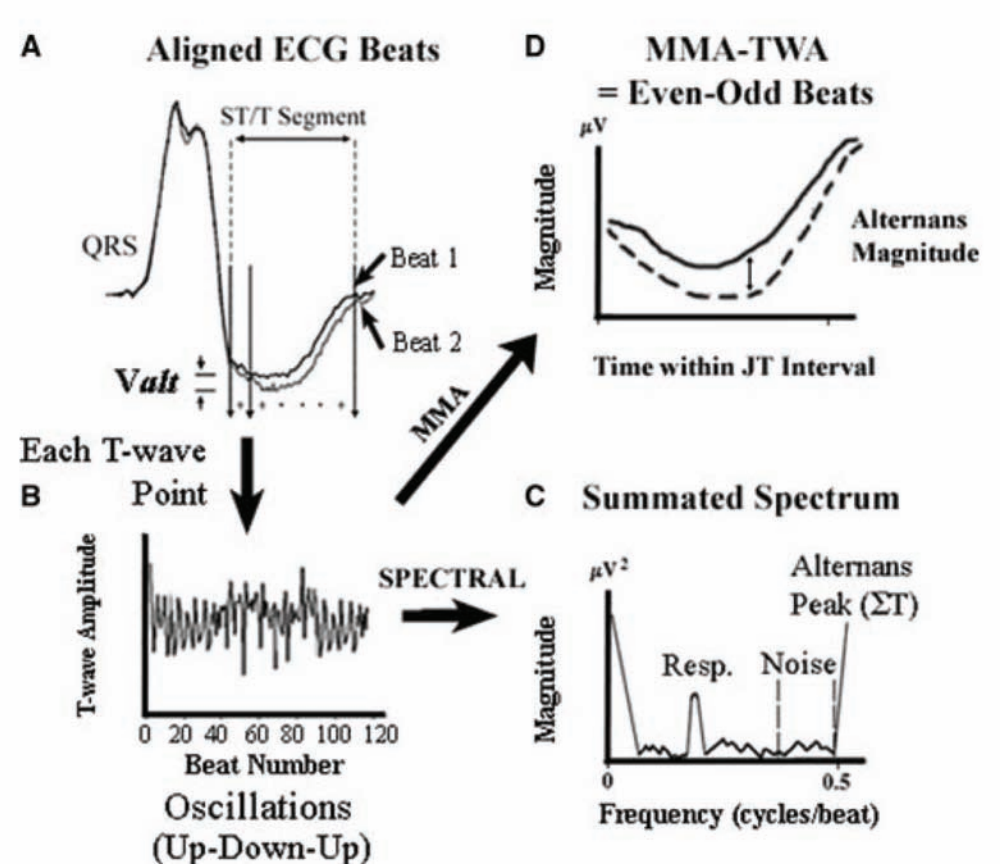

Figure 18 TWA Computation (A) Beats are aligned by QRS complexes. At each successive timepoint- in the aligned T-waves (arrows) (B) Beat-to-beat oscillations reflect alternans at each timepoint (C) Spectral Analysis applies fast Fourier transformation to yield a power spectrum in which alternans is the peak at the frequency of half the heart rate (0.5 cycles/beat). (D) MMA analysis uses a nonlinear filter to quantify the maximum difference between the means of 'even' versus 'odd' beats in an alternating sequence. Figure reproduced with permission, from [Pantelopoulos. A, et al, 2010]

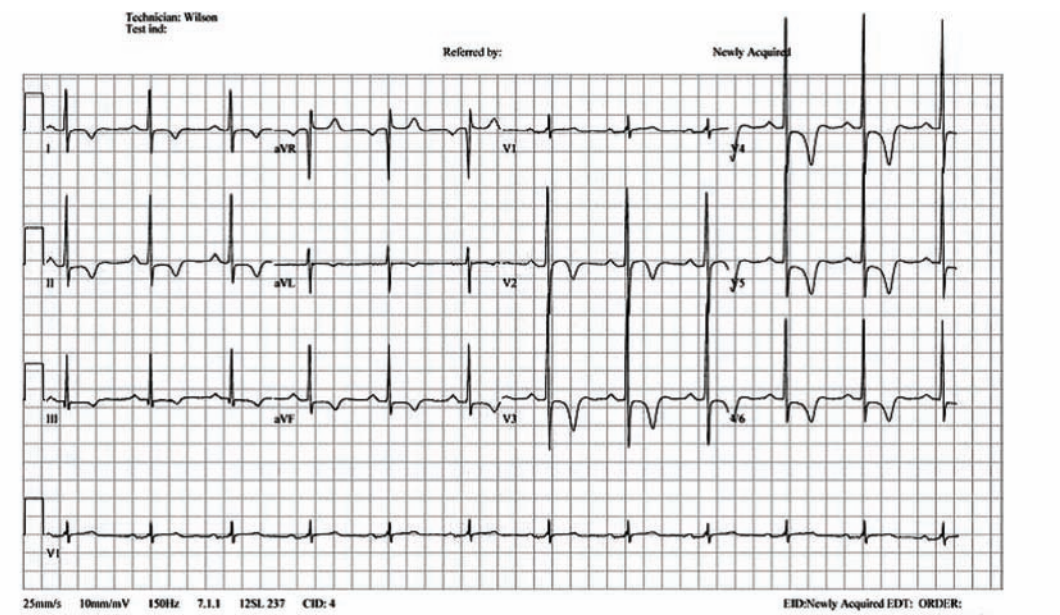

Figure 19 T-wave inversion in leads I, II, III, aVF, V2–V6 and ST-segment depression in leads II, aVF, V4–V6 in a 31-year-old asymptomatic professional soccer referee during cardiopulmonary exercise. The subject had no family history of SCD. Reproduced with permission, from [Saroj K.L et al, 2001]

wave loop morphology. This makes it a direct measure of the regional heterogeneity of myocardial repolarization, which has the predisposition to re-entry arrhythmias.It is known that potassium, calcium, magnesium and metabolic acidosis are important factors for the overall electrical stability of the myocardium to ensure normal cellular excitability, impulse propagation and regular ventricular recovery. Large amounts of or rapid removal of potassium, low calcium dialysate, intracellular magnesium overload, iron overload and rapid bicarbonate gain (metabolic acidosis) are the factors that increase *QT* dispersion in dialysis patients [Wu *et al.*, 2005].

4. Monitoring Systems

4.1 Commercially Svailable Monitoring and Recording Systems – Neurological and Cardiovascular

All ECG, EEG, EOG and EMG monitoring systems in the market are mostly defined by the type of signal acquisition and storage system they use. The recording and acquisition of signals is done by a multichannel desktop recording, display and monitoring system, or its handheld version, a portable data logging device Holter monitor. A majority of systems can be classified into these two categories. Modern multichannel desktop recording systems can connect to the physician's office from a remote location with the help of Ethernet connectivity or by a wireless network to a nearby workstation for easier workflow. Further advancement has allowed the inclusion of automatic triggers that can alert the nursing staff in the hospital but it is still confined to the hospital bed. The Holter monitoring system is the only commercially available multiple lead ambulatory measurement system and it performs only data logging. A list of noteworthy commercialized ECG recording technologies has been listed in Table 4.

In recent years, these monitors have been equipped with an event recording functionality that allows for automatic or manual logging of the time-of -the- event onset, while continuously recording the ECG signals. In addition to this, the Holter can be interfaced with wireless electronics to achieve ambulatory monitoring. This measure has challenges such as a short battery life and a large data volume for transmission.

Most EEG recordings for diagnostic purposes are performed in hospitals or other clinical settings. Commercially available ambulatory or out- of-hospital recording platforms for EEG, EOG and EMG are primarily intended for sleep studies that need to be performed at home. A brief list is provided in Table 5.

A survey of existing monitoring and diagnostics indicates that there are a few systems for ECG, EEG, EOG and EMG, which facilitate at- home and

Table 4: Commercial ECG recording platforms

Manufactures	Product Name	Total numberof channels	Storage	Wireless
Phillips	Page writer TC50 EKG	12 channels of ECG	USB memory stick (upto 16 GB)	No
GE Healthcare	MARS Ambulatory ECG System (SEER 12,	3-12 channels of ECG	1 GB internal and optical DVD storage SEER light)	No
medGadget	TruVue	1 channel ECG, 1Plethysomopragh	N/A	Yes
Imec	Secure Digital Input Output	1 channel ECG	16GB	Yes
AliveCor®	AliveCor	1 channel ECG	16GB	Yes
Phillips	EASI (Philips DigiTrak XT)	4 channel ECG	256-512 MB	No

Table 5: Commercial EEG, EOG and EMG recording platforms

Manufactures	Product Name	Total numberof channels	Storage	Wireless
Philips/ Respironics	Alice PDx	21channel with optional ECG and EEG	1GB SD card	No
Embla	Embletta X100	12-channel with X 100 proxy	128MB internal memory	No
Compumedics	Somte PSG	16-channel	2GB Compact Flash	Bluetooth
Compumedics	Siesta	32-amplified channel	Compact Flash	Siesta's Ethernet radio link
Cleveland Medical	Sleep Scout	9-channel	SD card	2.4-2.484 GHz
ResMed	ApneaLink Plus	4-channel	15MB internal memory	No
CareFusion	Nox-T3	14-channel	1GB SD card	No

ambulatory monitoring. With the help of the post processing of recorded data and/or the real time processing of wirelessly transmitted data at a centralized location, it is possible to perform a diagnosis. However, these systems make ambulatory monitoring an added chore rather than a fully automatic process which would be possible with RPM systems. The electrodes need to be replaced after the conductive gel dries up or after a prolonged exposure to sweat. Applying these electrodes requires the help of a clinical technician, and dry electrodes require mechanical appendages such as straps to keep them in place. In addition to this, ECG systems have wire-outs from the electrodes to the recording equipment. Unless tucked in and taped as in the case of the Holter monitor, the wires limit the movement of the patient.

The systems listed in this section do not use or, reluctantly, use wireless technology. This means that the data need to be brought to the hospital for post processing and administration of therapy. These intermittent treatments are brief and expensive supervised episodes [Go *et al.*, 2013, Rawles, 1996]. Therefore, well defined wireless communication is required in wearable monitoring systems to provide continuous and remote healthcare in an affordable way.

4.2 Wireless Health Monitoring: State-of-the-art

Textile-based nano-biosensors can be combined with flexible wireless sensors and can be incorporated in garments of daily use e.g. a vest, brassiere, head band or skull-cap. The sensors can combine with a wireless health diagnostic system made of embedded wireless networking devices which can communicate with a smart phone. This enables the connection of nanosensors to cloud computing, via a smart phone, to fundamentally advance remote cyber-enabled health care.

The challenge in designing wearable and wireless healthcare devices is two-tiered. The *First*, is to design sensors that are small in size and do not require any additional preparation on the part of the wearer, such as, cleaning the skin with an alcohol swab or shaving the area to remove any hair that might interfere with the measurement of biopotential signals. The *Second* is the wireless communication architecture that provides both easy access to patient data and is a turnkey sort of solution with minimal effort required for the initial setup.

4.2.1 Wireless Communication Implementations

Wireless devices follow standard communication protocols to interface and connect to each other. The established communication standards are IEEE 802.11 (Wireless Local Area Network (WLAN), IEEE 802.15.4 from which ZigBee™ is derived, IEEE 802.15.6 which is Bluetooth™ and Custom radio frequency (RF) transceivers. The choice between

wireless protocols for the development of a wearable wireless health monitoring platform largely deals with the complexity of the connection, power consumption and the scalability of the application from a single to a multiple user system.

WLAN, Wi-Fi based systems and Wi-Fi-Bluetooth integrated systems have been demonstrated [Yu *et al.,* 2006] but Wi-Fi consumes as much as four times the power consumed by Bluetooth and hence is not an energy efficient solution. ZigBee™ is an attractive protocol as far as connection stability, link layer retransmit in the case of data loss and a large range of network configurations are concerned, but the data rate is much lower than that of Bluetooth™. Moreover, ZigBee™ is not available on standard portable devices. Custom RF transceivers do not have limitations on the data rate and consume less power than Bluetooth™ but additional hardware is necessary to connect than to standard devices. Thus, Bluetooth™ is ideally suited for pervasive wireless healthcare devices because of the new ultra low power connection profiles, high data rates of up to ~3Megabits per second (Mbps) and standard availability on all portable electronic devices.

The ultimate goal for all communication architectures is to provide a means of storing the large quantity of real time patient healthcare data in a remote server and providing emergency warning mechanisms wherein abnormal data is automatically identified and a warning is sent to hospitals, physicians and the patient as well. Based on these requirements the solutions proposed thus far have been:-

1. A Custom RF transceiver sends data to a PC with a plug in RF transceiver and the PC processes and uploads the data [Huang *et al.,* 2009].

2. The ZigBee™ based approach which is similar to custom RF in that connectivity is to a PC or a customized receiver module that has a Wi-Fi-ZigBee™ combination chip that directly uploads to a server [Varadan *et al.,* 2010]. This has the potential of a scale up in a setting such as home and local area network (LAN) hotspots.

3. A Bluetooth™ based smart phone relay with local signal processing and data relay through a Global System for Mobile Communication (GSM)/General Packet Radio Service (GPRS) [Lee *et al.,* 2007]. This solution truly facilitates wearable health monitoring systems applications.

4.2.2 Sensor to Wireless Module Connectivity

The integration of sensors and the signal conditioning and wireless modules in wearable platforms can be achieved through three strategies.

1. Connecting the sensors through wires to a small module that incorporates signal conditioning, amplification circuits as well as a wireless transceiver.

2. Connecting each sensor to a small wireless module that acts as an independent node – Body area Network (BAN)

3. Integration of various sensors on a garment and using conductive threads and yarn to carry power and signals from the sensors to a small signal conditioning and wireless transceiver module.

Wired

This is the first generation of portable healthcare devices in which systems for POC monitoring consisted of wired sensors that the patient needed to mount manually (Figure 20).

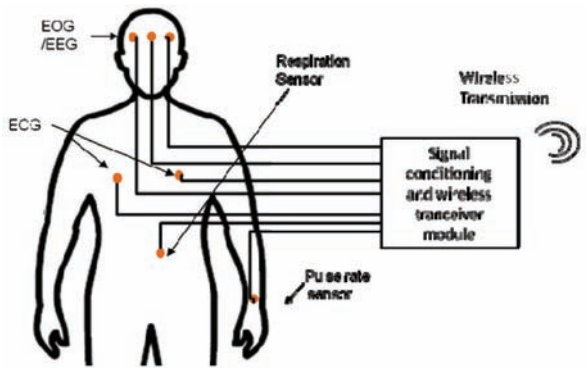

Figure 20 Schematic of sensors using wires to connect to a single amplifier, signal conditioning and Radio Frequency Transceiver module

Complete health monitoring needs multiple sensors: bioelectric signals like electrocardiogram (ECG), Electromyogram (EMG), Electroence

phalogram (EEG), Electrooculogram (EOG), light absorption based sensors for pulse oximetry, pressure flow sensors for air flow measurement, and strain sensors for respiration effort measurement. Each sensor has to be wired through regular insulated wire or shielded wires in the case of biopotential signals. The wireless communication module uses custom data transmission hardware and software that does not easily integrate into a patient's quotidian life—an individual has to carry a special device for data collection. This approach is not user- friendly. Although a significant improvement in terms of portability is achieved, the sensors used in a majority of these systems are not wearable. Figure 20 shows a schematic of these wired sensors.

Body Area Network (BAN) Concept for Healthcare Devices

BAN is a network of independent wireless nodes that span the personal space of a user Figure 21. Various wireless protocols have been used to implement BAN. The state of the art standards in BAN in wearable sensor systems is discussed in detail in [Pantelopoulos *et al.*, 2010]. The ultimate objective is to have independent sensors for physiological signals like Electrocardiogram (ECG), Electroencephalogram (EEG), Electrooculogram (EOG), Electromyogram (EMG), Pulse rate, Blood oxygen saturation (Pulse Oximetry and Photoplethysmography), temperature and respiration that have wireless transmitters sending data to a single receiving station which may be a Personal Digital Assistant (PDA), a tablet Personal Computer (PC), a PC, a smartphone or a custom receiver unit. The various wireless communication protocols used are Bluetooth™, ZigBee and custom communication protocols for low power transmission of data. The truest embodiment of this concept will have all body- worn

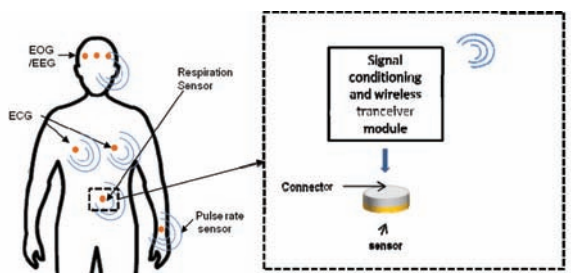

Figure 21 Illustrates the concept of Body Area Network of wearable sensors incorporated in band-aid

sensors (slaves) communicating with a single receiver unit (the master) and transmitting time-synchronized data in real-time. Figure 22 presents a schematic of the concept.

5. Neurological Disorder Monitoring by Wearable Wireless Nano- Bio- Textile sensors

This section presents textile- based wearable nano-biosensor systems that can measure neurological signals and identify anomalies for the diagnosis of targeted neurological disorders. These intended applications include chronic disorder monitoring, monitoring for safety and rehabilitation, and for improved quality of life.

A range of specific disorders can be identified and diagnosed with bio potential signals such as electroencephalography (EEG), electrooculography (EOG) and electromyography (EMG), because of their rooted significance and origin. By measuring and analyzing these bio potential signals, certain neurological disorders can be detected or diagnosed. Several applications such as sleep disorders, drowsiness and brain machine interface based on these bio potential signals detected by textile based analog nano- sensors are described in the following sections.

5.1 Wireless Telemedicine System for Diagnosing Sleep Disorders – The Home Sleep Test (HST)

Sleep disorders are related to sleep patterns and are characterized by disturbances in the amount, quality or timing of sleep. There are about 88 recognized sleep disorders. According to the International Classification of Sleep Disorders, the sleep disorders are classified as dyssomnias, parasomnias, sleep disorders associated with other disorders, proposed sleep disorders [Levi-Montalcini, 2007]. According to the National Institutes of Health (NIH), 50 to 70 million Americans suffer from sleep disorders and sleep deprivation [Shen *et al.*, 2006]. The short-term effects of sleep disorder are morning headaches, excessive daytime sleepiness, short-term memory loss and depression. The cumulative long-term effects are associated with heart failure, stroke/ transient ischemic attack, Type 2 Diabetes, and

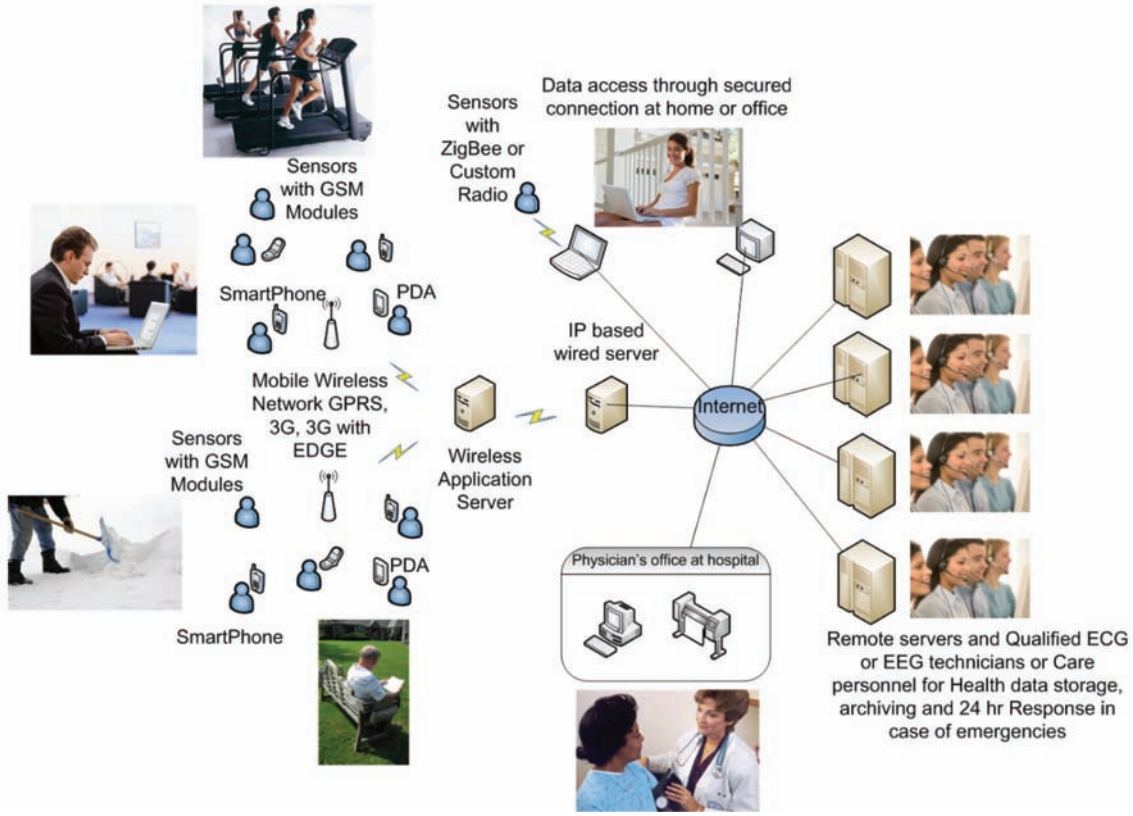

Figure 22 Textile integrated sensor for relaying sensor data over the internet to a remote server for diagnostics by doctor.

Hypertension [Young *et al.*, 1993]. Apart from chronic physical risks, undiagnosed sleep disorders lead to serious consequences from a social perspective. Undiagnosed sleep disorders impose over $22 billion in unnecessary health care costs.

Polysomnography (PSG) is a standard approach to the monitoring of sleep patterns. These recorded physiological signals are scored over the epoch by a sleep specialist or an auto-scoring program into one of six stages (Table 6), wake, rapid eye movement (REM) and non-REM stages (NREM). There are four types of sleep study devices according to the Center for Medicare & Medicaid Services (CMS) and the American Academy of Sleep Medicine (AASM). Type I PSG measures almost all kinds of physiological signals with around 20 sensors and is performed by a sleep technologist in a sleep lab. Thus, it provides accurate diagnosis. The cost of performing a PSG ranges from $1,000 to $5,000 and the waiting time from a few weeks to more than a year because of the currently insufficient capacity of sleep laboratories [Flemons *et al.*, 2004]. In addition to that, the patient has to spend a night at the sleep laboratory, which can be an inconvenience that may even affect the results of the test.

The Home Sleep Test (HST) is performed at home in the comfort of the patient's own home and there are no long waiting lists to schedule the exam. The HST records and saves the sleep data to the internal or external memory. Notwithstanding providing convenient and cost-effectiveness, it has no real-time monitoring and a limited amount of physiological information. Recently introduced wireless HST devices save the sleep data to a local server wirelessly. Most of them adopt Bluetooth, ZigBee or their own protocols as a wireless communication method over industrial, scientific and medical (ISM) bands. The wireless communications used to build wireless personnel are network (WPAN) or wireless body area network (WBAN) to save or monitor the sleep data. However, the wireless network area is limited to the personal area or body area. The real-time monitoring of the physiological signals at remote locations for sleep disorders can be achieved by combining two

Table 6 Biopotentials in sleep disorders according to the Rechtschaffen and Kales standard [Wessberg. J, et al, 2000]

Physiological Characteristic	Wake Stage	Stage 1 NREM	Stage 2 NREM	Stage 3 NREM	Stage 4 NREM	Stage REM
EEG	Parieto-occipital alpha waves (8-13 Hz) more than 50% of the mixed with fronto-central beta rhythms (> 13 Hz)	Alpha waves decrease to less than 50% of the epoch: theta (4-8 Hz) and beta rhythms occur, may have vertex waves	Sleep spindles (approximately 12-14 Hz) and K complexes lasting at least 0.5 sec; delta waves of 2 Hz or less measuring 75 uV or more occupying < 20% of the epoch	Delta waves of 2 Hz or less measuring 75 uV or more occupying 20-50% of the epoch	Delta waves of 2 Hz or less measuring 75 uV or more occupying > 50% of the epoch	Theta waves; saw tooth waves; beta rhytms
EOG	Waking eye movement	Slow eye movement	Silence	Silence	Silence	Rapid Eye Movement
EMG	Elevated	Elevated but less than in awake stage	Mildly decreased	Mildly decreased	Mildly to moderately decreased	Markedly decreased to absent

wireless communication standards or using the mobile communication network. The concept of combining two wireless communication standards is extending WPAN/WBAN to WAN. Therefore, one wireless communication standard is for building WPAN/WAN and the other wireless standards are for WAN.

The sections hereafter describe the wireless HST devices which support the real-time monitoring of sleep data at remote places by using a combination of wireless communication standards.

System Description

The system mainly consists of sensors, a wireless sensor electronic unit, a wireless receiver unit and a monitoring unit. The system measures 5 biopotential signals to evaluate the sleep stages; 2x EOG, 1x EMG and 2x EEG. The receiver unit adopts two wireless communication standards, Wi-Fi and Zigbee. The combination of two wireless standards in the receiver unit allows us to build WPAN and extend the WPAN to WLAN/WAN. The sensor electronic unit sends the sensed 5-channel signals 2x EOG, 1x EMG and 2x EEG to the receiver unit through a Zigbee network. The receiver unit then retransmits to the monitoring unit or remote server through the Wi-Fi network. Figure 23 shows the data flow of the system [Varadan *et al.*, 2010].

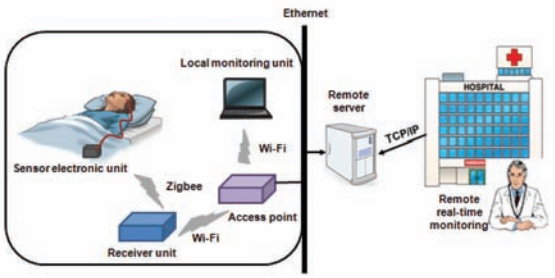

Figure 23 Data flow of the wireless telemedicine system for diagnosing sleep disorders

As dry electrodes, nanostructured textile-based electrodes or gold nanowire electrodes can be used instead of a conductive gel to overcome the drawbacks of wet silver-silver chloride electrodes as mentioned previously i.e. Figure 24 shows both the dry electrodes. The main functions of the wireless sensor electronic unit are data acquisition, data processing, and data flow

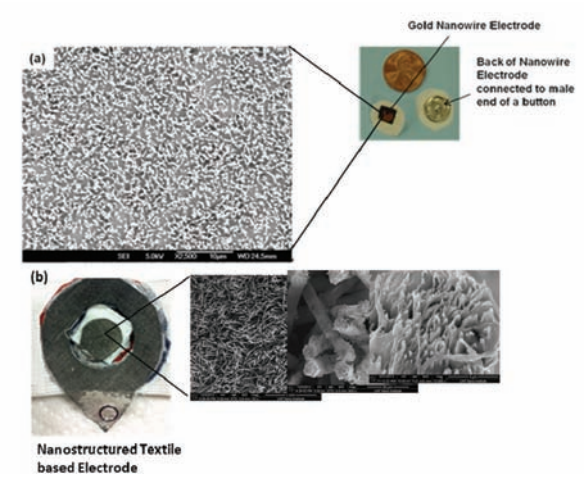

Figure 24 (a) Vertically aligned gold nanowire electrodes, (b) Nanostructured textile nano-biosensor

management and data transmission. The wireless sensor electronic unit consists of an amplifier module, a data acquisition/process module and a Zigbee wireless module.

The raw physiological signals from the sensors are very weak, ranging from micro-volts to milli-volts, and are contaminated by noises, especially 50/60 Hz power line interference. Therefore, the signals need to be amplified and filtered to improve the signal to noise ratio. The biopotential signals for sleep studies are differential signals. The body impedance and contact impedance between the skin and the electrodes might vary under different skin conditions leading to impedance mismatches. Therefore, an amplifier should have a high common mode rejection ratio (CMRR) and high input impedance to maintain signal integrity. The amplifier module has 5-channels for 2x EOG, 1x EMG and 2x EEG. The gain and bandwidth of each channel were tuned according to the AASM manual [Iber *et al.,* 2007]. The amplified signals are digitized using an analog to digital converter (ADC) on the microprocessor.

Finally, the signals are transmitted to the receiver unit by the Zigbee module. The output of the ADC is transferred to the ZigBee module through a Universal Asynchronous Receive/ Transmit (UART) interface. The data from the microprocessor are transmitted to the wireless receiver unit through ZigBee. The data received by the receiver unit are reconstituted as packets with a sequential hex code including a node number, sampling rate, the number of channels and the data according to the defined communication protocol. These packets are saved in the data buffer temporarily and transmitted when a data request is received from a PC or a remote server. The ZigBee interface routinely checks the wireless connection between the sensor electronic unit and the receiver unit, and then transmits the sleep data to the receiver unit. This is done to ensure recovery from lost wireless connections. The wireless sensor electronic unit uses a 3.7V poly lithium battery as a power supply (Figure 25).

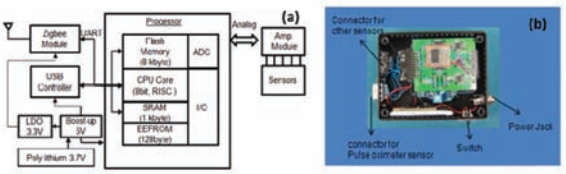

Figure 25 (a) block diagram and (b) image of the wireless sensor electronic unit

While the function of the sensor electronic unit is to build the wireless personnel area network with ZigBee, the role of the receiver unit is to extend the ZigBee network to the wireless local area network with Wi-Fi. The sleep data needs to be monitored at remote places. Therefore, the network should be extended to use Internet through Wi-Fi because ZigBee is not as prevalent as Wi-Fi. The processor board in the receiver unit consists of two wireless modules, the ZigBee and Wi-Fi module, a 16 MB SDRAM as a buffer for sensor data, a 64 MB NAND Flash memory for the storage of programs, a 32-bit microcontroller and an Ethernet controller. The receiver includes the ZigBee and Wi-Fi module management and the server management based on TCP/IP [Varadan *et al.*, 2010]. Figure 25 shows the block diagram and image of the wireless receiver unit and Figure 26 shows the data flow in the wireless receiver.

Two electrodes were placed on the left lower and right upper side of the eyes to measure 2-channel EOG. One of the electrodes was placed on the chin to measure EMG and to detect the grinding of teeth or mouth movement. The last two electrodes were placed on C3 and O2 positions on the scalp according to the international 10-20 system. The reference electrode to measure the differential biopotential signals was placed on the left ear lobe. Figure 27 shows an image of a subject

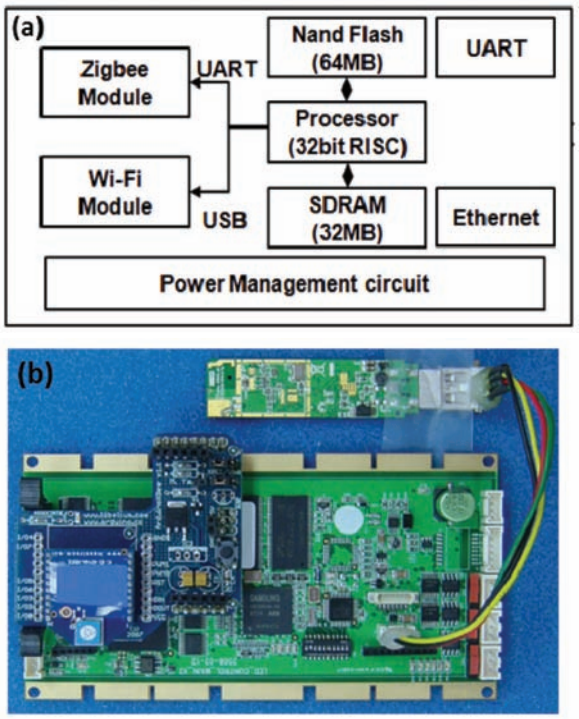

Figure 26 Data flow in the wireless receiver unit

under a sleep study with the proposed system and the GUI of the monitoring utility program developed using MATLAB (Matworks, Inc, Natick, MA, USA).

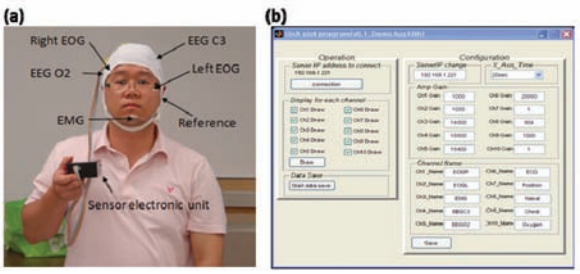

Figure 27 Experimental test set-up for the system with Zigbee and Wi-Fi; (a) image of a subject under experiment and (b) GUI of the monitoring utility program

Figure 28 shows the measured and recorded biopotential signals using this system. In the case of EOG, five different types of eye motion, blinking, left, right, up and down movement of eyeballs, can be detected to emulate REM and the wakeful sleep stage. The left and right EOGs show an opposite polarity of slope due to the placement of the electrodes over the reference electrode. EMG reflects the movement of the chin. The EEG acquisition performance can be verified by discerning between beta waves and alpha waves. Beta waves are associated with normal waking

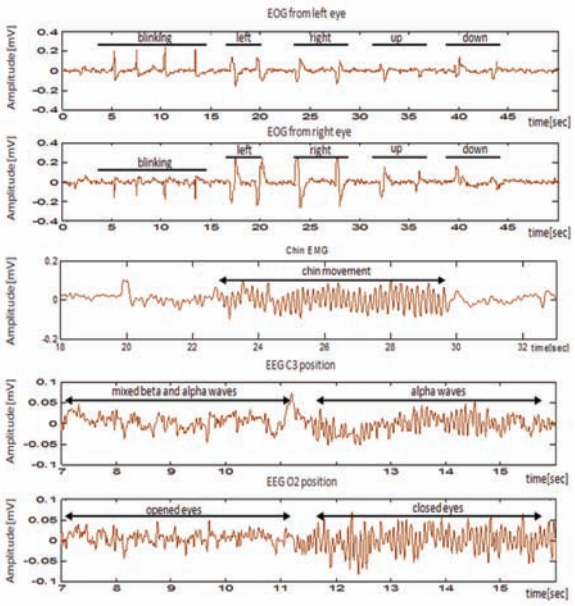

Figure 28 Monitored EOG, EMG, EEG from the wireless telemedicine system for sleep study

consciousness and Alpha waves with wakeful relaxation with eyes closed. By opening and closing the eyes alternately, the changes of brain waves can be observed. The EEGs from the C3 and O2 positions show that alpha waves are dominant when the eyes are closed. The EEG from position O2 shows stronger alpha waves than from position C3 even though both the channels of the amplifier are set to the same gain. It verifies that the alpha waves predominantly originate from the occipital lobe during wakeful relaxation with closed eyes.

In a case study on a human subject from 10 pm to 4 am, 5-channel signals were monitored and recorded in real-time [Varadan *et al.*, 2010]. The EEG signals are plotted in Figures 29-31. Based on the criteria specified in TABLE 6, a transition between sleep stages can be seen in the EEG data from C3 and O2. This shows that a wireless telemedicine system for diagnosing sleep disorders can address the need for the efficient extension of the network to provide remote monitoring in real-time. The dry electrodes and a scalable WPAN-WLAN wireless technology will foster more convenient and accurate diagnosis of sleep disorders.

5.2 Drowsiness Monitoring: A Textile Based Nano-biosensor System Head band with GSM

Wireless wearable textile based nano-biosensor systems can also be useful in improving

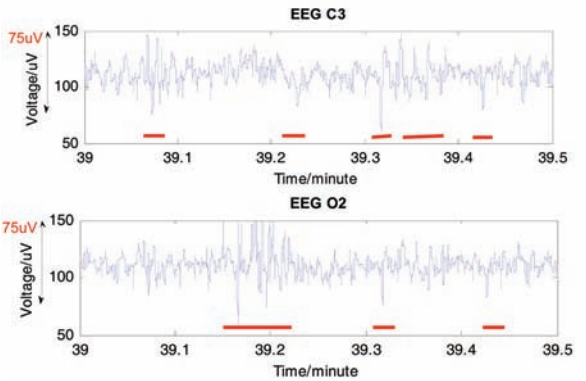

Figure 29 This epoch illustrates the beginning of transition from Stage 1 to Stage 2. Vertex sharp waves are very prominent. In the beginning of the epoch, theta and alpha waves are dominant. In the middle of the epoch, there is a K complex. End of the epoch, delta waves less than 2 Hz are shown.

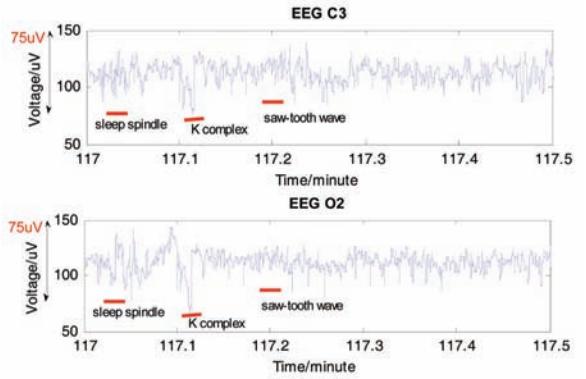

Figure 30 This epoch illustrates the Stage 3. Acceptable high amplitude, slow wave activity occupies between 20% and 50%.

safety. This application addresses a condition that interferes with human performance and can become an occupational hazard. Drowsiness is defined as the onset of sleep or the precursor for sleep. For instance, the transition state from wakefulness to sleep under undesired circumstances (in most cases) is defined as drowsiness. It can also be referred to as an intervening process in concentration and attention. Additionally, fatigue or drowsiness is also referred to as the psychological disability which results from various sources and origins [Saroj *et al.*, 2001]. Drowsy driving is one of the most common reasons for road accidents. National Highway Traffic Safety Administration (NHTSA) estimates that approximately 25% of police-reported crashes involve some form of driving inattention - the driver is distracted, asleep or fatigued, or otherwise "lost in thought" [Ranney *et*

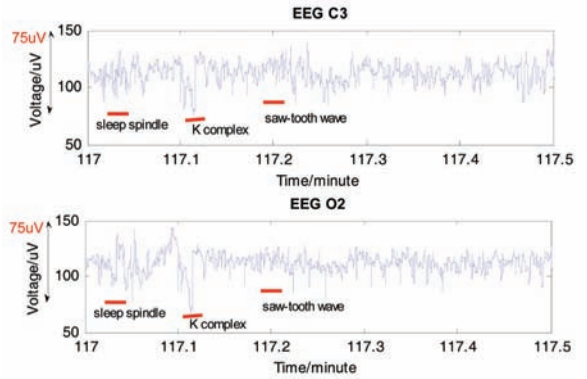

Figure 31 This epoch illustrates a transition between Stage 2 and Stage REM. In the beginning of the epoch, there is sleep spindle followed by a K complex. Following the K complex are saw-tooth waves which herald the appearance of REM. The last half of epoch shows relatively low voltage, mixed frequency.

al., 2000; ETSC, 2001]. The 100-Car Naturalistic Study [Neale *et al.*, 2005] recorded the activities of 241 drivers over the course of 12 -13 months and found that 78% of the crashes and 65% of near crashes had one form of inattention as a contributing factor.

The Monitoring of people like security personnel, drivers, shift based workers and custodial workers who need to stay awake during the normal sleep cycle, and the prevention of people from falling asleep on wheels to avert accidents requires drowsiness monitoring systems. The Psychomotor Vigilance Test (PVT) [Robertson *et al.*, 2004], Epworth Sleepiness Scale, Maintenance of wakefulness test (MWT), Karolinska Sleepiness Scale (KSS), video monitoring, subjective reports and behavioral approaches are some of the tests performed to assess the quality of sleep from which an inference can be derived about attentiveness during a task [Nilson *et al.*, 1997].

These systems rely on biopotential signal approaches to discriminate between sleepiness and wakefulness. Primarily, biopotentials like ECG, EOG and EMG are collected through the electrodes by establishing a skin-electrode contact. Methods like sample entropy and phase synchronization are used in this process of discriminating between sleep/wakefulness. However, a real time and accurate monitoring system to detect drowsiness and classify sleepiness/wakefulness or drowsiness/alertness becomes highly essential for continuous monitoring

if the system has to avert road collisions. [Ramasamy *et al.,* 2013; Lin *et al.,* 2005; Jap *et al.,* 2009]

Considering the preceding parameters as factors of a reliable and a real time monitoring unit, a flexible headband equipped with sensors and a GSM wireless transmitter that can communicate with a receiver at a remote location was built (Figure 32). A Textile based nano-biosensor is placed in such a way that it is in contact with the forehead for monitoring the frontal cortex of the brain. The sensor was designed to detect raw biopotential signals, which are a combination of EEG and EOG [Ramasamy *et al.,* 2013]. The amplifier and an A/D converter circuit feeds the digitized signal to a GSM module, which can send data to a remote server for real time monitoring and detection of a person's level of drowsiness. The usage of the GSM module provides an advantage over the communication distance as it covers longer distances as compared to Bluetooth and ZigBee. This attribute is important in applications for personnel with high risk or field jobs.

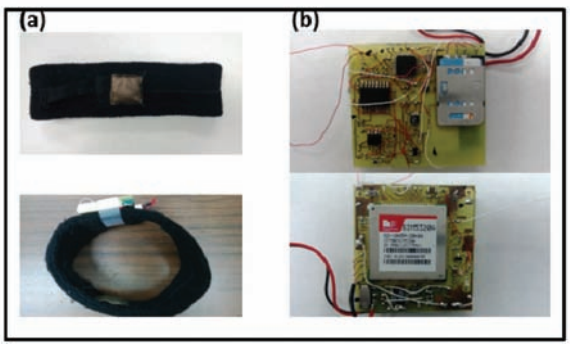

Figure 32 (a) Front and top view of the headband (b) front and backside of the processing module

This system correlates the EEG and EOG signals to facilitate the interlinking of eye blinks and the discrimination of alpha and beta waves. In the EEG signal, alpha wave dominance is present when a person is relaxed and beta waves are dominant when the person is attentive. Similarly, an assumption that a person falling asleep will have a slower eye blink rate than an attentive or a normal person is also made. Subsequently, the pace at which the eyes blink is measured, where the difference in pace and waveform during slow and normal blinks is analyzed. Correlating all these features extracted from EEG and EOG is finally used to estimate the condition of the person. [Ramasamy *et al.,* 2013]

The back end of the module consists of software at the receiver end which is programmed to extract the features from the EEG and EOG signals. Specific features from which sleep can be detected are extracted in the software and it pops out a warning signal when the driver falls asleep. The rate of eye blinks from the EOG signal and the peak values from Autoregressive Power Spectral Density (AR-PSD) of the brain signal in the alpha frequency band are correlated to estimate the condition of the person. The receiver side software is programmed to perform feature extraction, AR-PSD of the signal, and improving the signal quality to adapt the processing strategy and parametric analysis. These separate results are then correlated in the main server program of the software according to the decision criteria, which are based on the initial set of experiments [Ramasamy *et al.,* 2013].

Initial experiments, as shown in Figure 33, are conducted to get ARPSD values fixing the decision criteria. It shows that the measured values clearly indicate that closed eyes have the highest and open eyes have the lowest value. Similarly, Figure 34 shows the average values obtained over a series of test cycles.

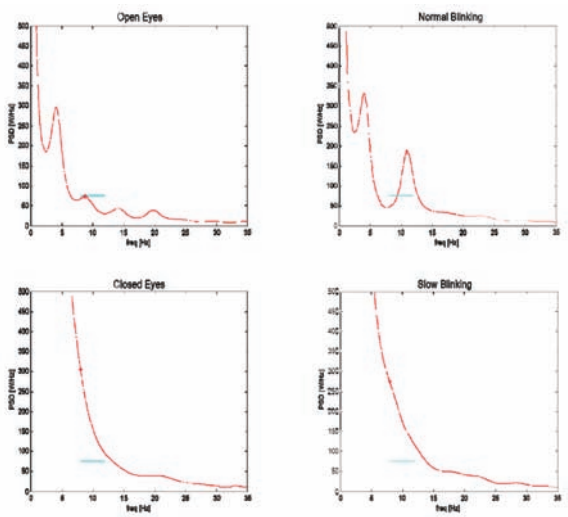

Figure 33 AR-PSD values depicting open eyes, normal blinking, closed eyes and slow blinking.

Upon a comparison of the test results of the flexible head band system on a real time driving simulator and PVT (Table 7), it was observed that an increase in the number of hours of sleep drastically worsened the reaction time of each

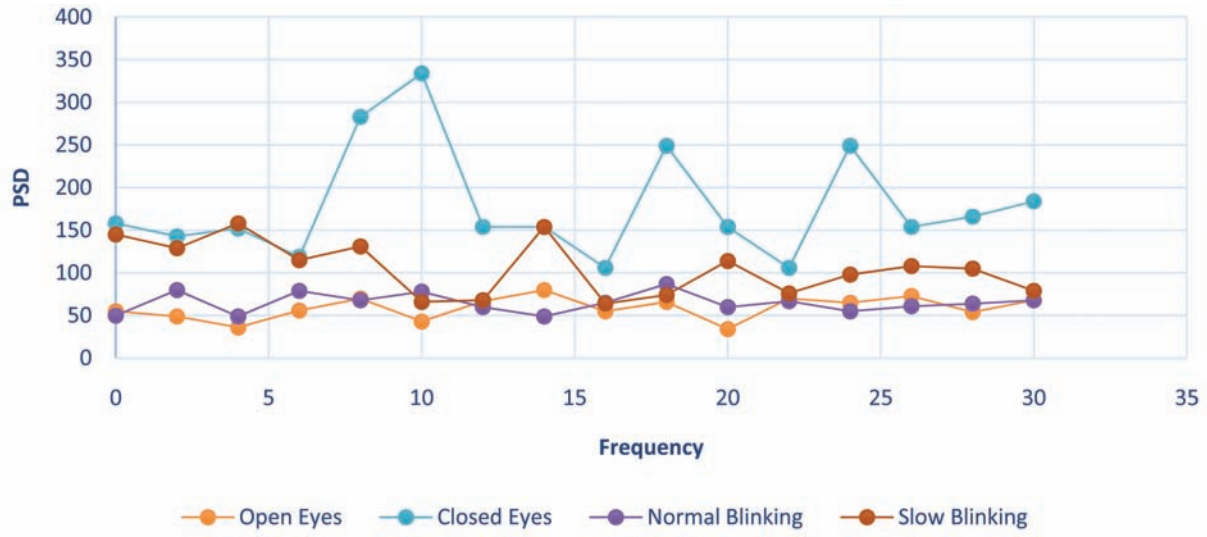

Figure 34 Cumulative results of (a) Peaks observed during normal blinks, close eye and slow blinks from EOG signal (b) AR-PSD values during open eye, closed eye, normal blinks and slow blinks from the EEG signal

Table 7: Comparison of test results of the flexible head band system and PVT

Condition the test subject	Observation of	Test 1	Test 2	Percentage of drowsiness calculated
Normal	Head band: Number of times drowsiness was detected out of 24PVT reaction time	2409 milli seconds	2397 milli seconds	12%
20 hours sleep deprived	Head band: Number of times drowsiness was detected out of 24PVT reaction time	12533 milli seconds	14578 milli seconds	54.16%
28 hours sleep deprived	Head band: Number of times drowsiness was detected out of 24PVT reaction time	21675 milli seconds	19654 milli seconds	83.25%

subject in any given cycle of a PVT test. Similarly, the number of times drowsiness was detected in the period of the PVT test proves that the flexible head band system detects greater drowsiness as the number of hours of sleep deprivation increased. Therefore, a correlation between the PVT and flexible head band system was derived. Hence, it was evident that the flexible headband system equipped a with textile- based nano sensor provided effective drowsiness and alertness discrimination. It is also evident from the analysis that the number of times drowsiness was detected increased when the reaction time of the subject increased.

5.3 Wearable Brain Machine Interface

Wearable nano-biosensor systems can be used in potential applications for interfacing the human mind with devices to operate them with thought and other neurological signals as cues. A brain machine interface (BMI) is a communication system that translates human thought into signals to control devices such as a computer application or a neuroprosthesis [Wolpaw *et al.*, 2002]. A BMI enables the brain to communicate with the external

world by deciphering the brain's activity. Hence, the assisting devices or systems using a BMI improve the quality of life in disabled people. In addition, a BMI has been proposed to replace humans with robots in the performance of dangerous tasks like explosives handling/diffusing, hazardous materials handling, firefighting etc.

Previous research projects have demonstrated the feasibility of a BMI with the invasive method by implanting intracranial electrodes in the motor cortex of monkeys [Chapin *et al.*, 1999; Wessberg *et al.*, 2000; Serruya *et al.*, 2002; Taylor *et al.*, 2002; Nicolelis, 2003]. Though an invasive BMI can use good quality brain signals, it is expensive and the implanting surgery may lead to undesirable side effects. A noninvasive BMI using electroencephalogram (EEG) signals are preferable for humans. EEG signals represent the electrical activity of millions of neurons in the brain. EEG has various properties and it can be used as a basis for a BMI: rhythmic brain activity, event-related potentials (EPRs), event-related desynchronization (ERD) and event-related synchronization (ERS) [Bashashati *et al.*, 2007]. Different rhythmic brain activities are shown depending on the level of consciousness. The brain waves are classified according to the frequency band: Delta (0.5-4 Hz), Theta (4-8 Hz), Alpha (8-13 Hz), Beta (13-30 Hz) and Gamma (30-100 Hz). These rhythms are affected by different actions and thoughts, for example, the thinking of movement attenuates or changes a typical brain rhythm. The fact that thoughts affect brain rhythms highlight the rhythmic brain activities that can be used for the BMI.

In general, the implementation of a BMI based on EEG signals requires the measurement of EEG, preprocessing, feature extraction, classification and device control. To measure EEG signals, textile based nano-biosensor electrodes are placed on the right places, typically according to the international 10-20 system. The preprocessing includes amplification, filtration and A/D conversion. In the feature extraction stage, certain features can be extracted from the preprocessed and digitized EEG signals in the frequency or time domain. The extracted features are the input of the classifier. The classifier can calculate the probabilities for the input belonging to each class. The signals are simply classified by threshold detection by the classifier. The output of the classifier is the input for the device control. The device control transforms the classification to a particular action of the device.

The wearable wireless brain-machine interface, shown in Figure 35, was designed to control a robot wirelessly [Oh *et al.*, 2012; Shyamkumar *et al.*, 2012]. The BMI controls the movement of the robot based on EEG and EOG signals. The EEG and EOG signals are captured with textile based nano-biosensor electrodes attached to a headband at positions across the forehead. This electrode placement is not a conventional placement meant for Electrooculogram (EOG) measurements. It was chosen because the signal response to the left and right movement of the eyes was strong enough to use as a command signal. Classified rhythmic brain waves are used to control the acceleration and deceleration or stopping of the robot by setting the threshold. The classified EOG signals from the left and right movements of the eye balls control the left and right direction changes of the robot.

Figure 35 Data flow of the wearable brain machine interface

The wireless transmitter module consists of a high gain biopotential amplifier to enhance the weak microvolt scale biopotential signals, a microcontroller that performs the analog to digital conversion and a Bluetooth module (Figure 36). The power source is a 250 mAh poly-lithium battery. The bio-potential amplifier is a three- stage amplifier with an overall gain of 65.44 dB and a 3dB bandwidth of 1.45Hz to 40 Hz set using active RC and Butterworth filters [Oh *et al.*, 2012; Shyamkumar *et al.*, 2012].

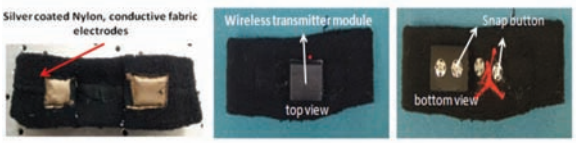

Figure 36 Images of the wearable sensing transmitter: (a) conductive textile electrode sensors on the headband, (b) top view of the wearable sensing transmitter snapped on the headband and (c) snap button male and female between module and the headband

The nano-biosensor electrode system measures the differential resting potential of the retina according to eye movements. If the eye is moved from the center position towards the electrode, this electrode sees the positive side of the retina and the opposite electrode sees the negative side of the retina. With this measurement method, all kinds of the eye movements are measured, left/right, up/down and the blinking movement. In this BMI system, left/right eye motion is used to take the decision of a robot turning left or right, hence, the other up/down and blinking motions are considered as noise. Thresholds of amplitude and time duration are used to remove the blinking and up/down motion. After removing the undesired eye motion signals, only the left and right waveforms remain. The two waveforms should be classified as left and right motion to send turning commands to the robot. The classification between two eye motions is done by investigating the polarity of waveforms. Left motion shows positive polarity and right motion shows negative polarity. Figure 37 shows the classification processes of left/right eye motion. The left and right motion signals are filtered with 5~15 Hz bandwidth to achieve sharp waveforms to process further. After filtering, integration is performed to make the signals smooth. The floor noises are removed by setting an adaptive amplitude threshold. The amplitude threshold is defined by 75 % of the peak values of the waveforms,. The cleaned waveforms by removing the noise floor are used to decide the command signals. As shown in Figure 37(e), finally, the left eye motion is coded to pulse amplitude 1 and followed by an amplitude 5 pulse. The Right eye motion is coded to the amplitude 5 pulse and followed by amplitude 1 pulse.

The Acceleration and deceleration of the robot are controlled by EEG signals. Among several brain waves, the alpha and beta waves are focused because they represent the mental states of attention and relaxation respectively. The received EEG signals are transformed into the frequency domain through Fast Fourier Transform (FFT) to investigate the brain waves. Each rhythmic brain wave is defined by the frequency band, and the mental states can be deduced by considering the amplitude change of the frequency band. To define the attention and relaxation level, the thresholds are set based on the ratio between the sum of AR power spectral density (PSD) of alpha and that of beta waves. Instead of taking the sum of AR PSD values, taking the peak AR PSD values over the frequency band was found to be more robust in noisy conditions. In an experiment to validate the EEG feature extraction algorithm, a subject was asked to be in an attention or relaxation mode by the experimenter and the calculated attention level was compared for accuracy with the actual mental states of the subject. The subject was asked to solve a series of quantitative problems to achieve the attentive state. Figure 38 shows the experiment result. As shown in the result, when the ratio of the peak PSD values of low beta and alpha was used, the accuracy rate was about 95 %.

Based on EOG and EEG feature extraction and classification algorithms, a whole system was

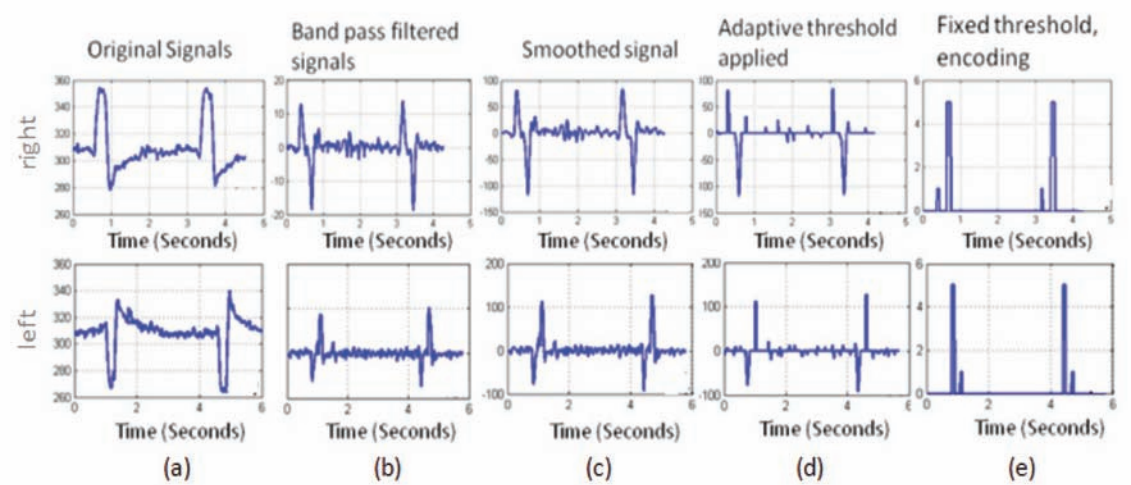

Figure 37 Classification process of EOG signals; (a) raw left and right EOG signals, (b) integrated signals, (c) filtered signals, (d) noise removed signals and (e) classified signals

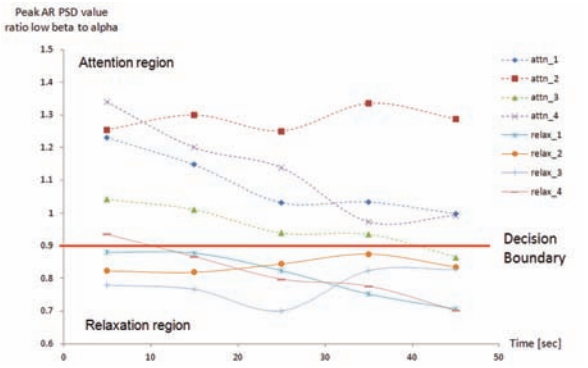

Figure 38 Experiment results of ratio the peak of the AR PSD value of low beta and alpha waves

implemented to control the robot. The speed of the robot was controlled by the attention and relaxation level extracted from EEG signals in the straight section and the changing direction of the robot was controlled by the left and right eye motions in the curved section.

6. Cardiovascular Health Monitoring

It is evident from Table 3 that ECG waveforms can be used in a number of diagnostic criteria that cover abnormalities in heart function, congenital conditions, predicting the onset of critical heart attacks (cardiovascular), strokes (cerebrovascular) or the autonomous nervous system.

Coronary heart disease, cardiovascular diseases and strokes are the leading causes of mortality in The United States of America as well as around the world. According to statistics by Centers of Disease Control and Prevention (CDC), cardiovascular or cerebrovascular disease was the most prominent cause of death in the United States of America. It was the cause of death in more cases than cancer, accidental injury, diabetes and infectious diseases [Go *et al.*, 2013]. Hence, an average American is more likely to die of a heart attack or a stroke than of cancer, accidental injury, diabetes or deadly infections such as HIV.

The point- of- care techniques suitable for ambulatory or out–of- hospital monitoring are non-invasive electrophysiological techniques: electrocardiogram (ECG) and electrical impedance tomography (EIT). Both techniques measure electrical activity and the properties of the cardiovascular system for long periods of time to detect abnormalities. In current medical practice, they are considered preliminary testing techniques. Any abnormalities detected in these tests are confirmed by in-hospital techniques: Echocardiogram, Cardiac Catheterization, Computed Tomography (CT) scan, Magnetic Resonance Imaging (MRI).

In the present form, ECG and EIT techniques use bulky instrumentation and constrictive conductive gel electrode based sensor systems that are not suitable for very long monitoring. Smart textile technology incorporates a textile-based dry and glueless sensor system in textiles of daily use such as vests, brassieres and under garments. The nanostructured surface of dry textile electrodes, discussed in this study, have improved sensor contact with the skin to match the performance of a conductive gel- based sensor system. In the point-of-care system of the future, ECG and EIT will serve as reliable diagnostic and monitoring tools for the detection of cardiovascular events in preventive medication and disease management. In combination with state of the art wireless technology, they will be able to establish a remote communication link between patient and doctor for telemedicine prescriptions and/or quick medical intervention in the case of an emergency.

6.1 e-Nanoflex: Smartphone Enabled Band aid Sensor

This application is a quintessential example of the implementation of textile based ECG nano-biosensors that can interface with smartphone technology. It has been demonstrated as a band aid named e-Nanoflex, which is made of a nano-biosensor with a Bluetooth™ module for communication with a smartphone [Varadan *et al.*, 2011].

Hardware System

The e-Nanoflex prototype was designed for the acquisition of ECG. A pair of nano-biosensor electrode pads was mounted on a wound dressing plaster to facilitate easy testing. The application was demonstrated with an electrode pair made of gold nanowire electrodes on a flexible Titanium foil as reported in [Yoon *et al.*, 2008] and textile-based nano-biosensors described in the section on *Nanotextured textiles as electronic sensors* (Figure 39).

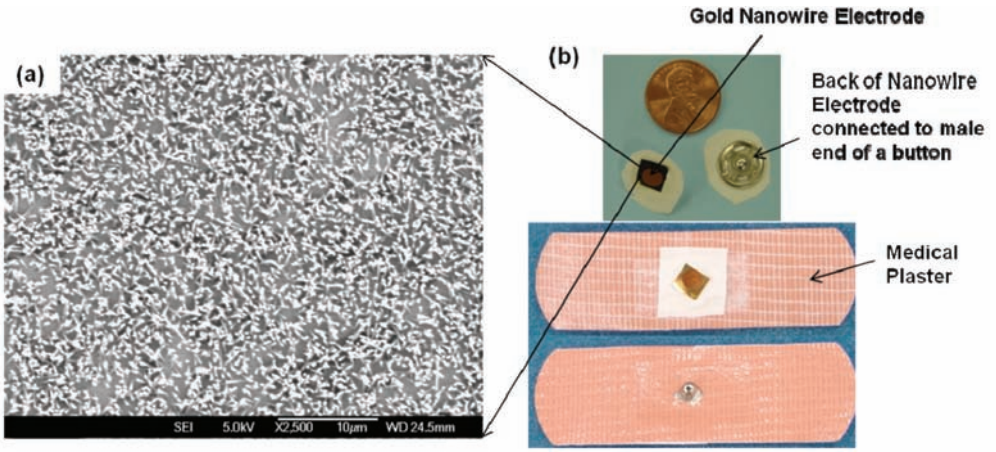

Figure 39 (a) Scanning electron microscope image of vertical gold nanowires (b) Shows the gold nanowire electrode packaged in a medical plaster

The ECG is a differential signal i.e. the signal is perceived as the difference in potential between two points on the skin in which one of the electrodes acts as a reference for the other. An amplifier was used to enhance the signal strength because the signal strength of ECG, at the level of the skin, is of the order of hundreds of microvolts. The Key attributes of the amplifier designed were a large common mode rejection ratio (CMRR), small input offset voltage and low input power consumption. The amplifier is designed in multiple stages. The instrumentation amplifier provides the first high impedance stage with a gain of 10 to avoid the amplifier's saturation due to an impedance mismatch. Analog filters with a pass band between 0.2 Hz and 70 Hz make sure the mismatch is not seen by the later high gain stages. Two more stages of non-inverting amplifiers are used to improve the signal quality. The amplified analog signal is then digitized by the ADC on the microprocessor at a fixed sampling rate of 200Hz. The microprocessor then communicates with the Bluetooth module using the Universal Asynchronous Receiver/Transmitter (UART) interface. The Bluetooth module continuously sends the data from the microprocessor to the data logging unit and the received data are then stored or processed by the host microprocessor of the smartphone. This application can be extended to a personal computer with a Bluetooth™ receiver [Led *et al.,* 2013].

The type of connection between Bluetooth devices, also known as profile, is chosen based on the kind of data that need to be sent from one device to another. For this application, the data are a series of digits which is the output from the microprocessor. The Serial Port Profile (SPP) was chosen because it supports the continuous transmission of data. The module basically broadcasts the SPP service, and any Bluetooth device, like a phone or a Bluetooth enabled PC that comes within range can securely connect to this device on that profile and start receiving the data if the correct passkey is entered.

One of the drawbacks of the SPP is that in case the data transmitted are not received by the data logging device, the data are not retransmitted automatically. This problem has been considered in detail in [Noueihed *et al.,* 2010]. The additional retransmit feature has to be implemented in the software to improve the reliability of an SPP connection. Alternatively, the introduction of a special profile for health devices called the Health Devices Profile (HDP), by the Bluetooth Special Interest Group (SIG) is expected to be more robust and suitable for this application than SPP.

ECG signal acquisition

This band aid type e-Nanoflex can be used for the measurement of single ECG leads. A Lead I ECG signal obtained from the sensor was plotted on a Smartphone in real time as shown in Figure 40. The frequency content of ECG is between 0.2 Hz and 70 Hz. The sampling rate was fixed at 200 Hz to satisfy the Nyquist-Shannon sampling theorem. A digital band pass filter with a bandwidth of 0.2 Hz to 70 Hz was implemented on the data logging device to improve the signal to noise

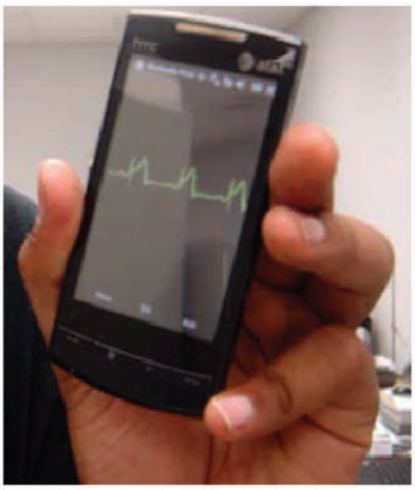

Figure 40 Shows Lead I ECG data displayed in real time on a Smartphone

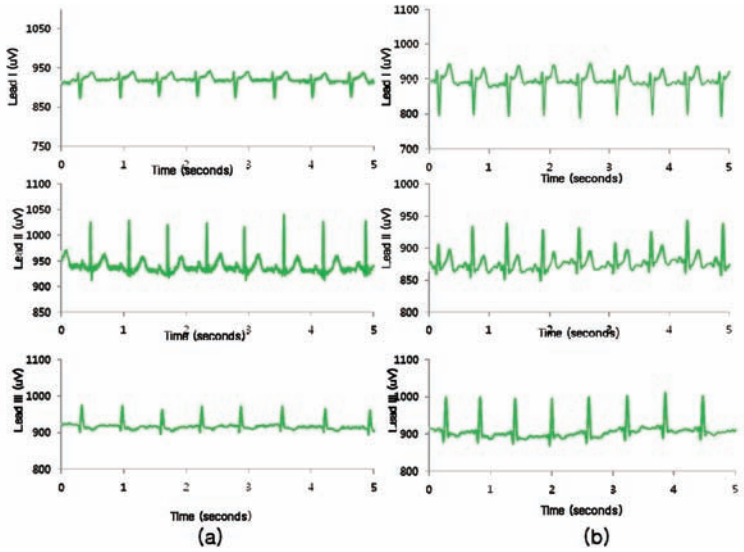

Figure 41 Three limb lead ECG acquired from e-Nanoflex sensor using (a) Commercial Ag/AgCl electrode (b) Gold Nanowire Electrode

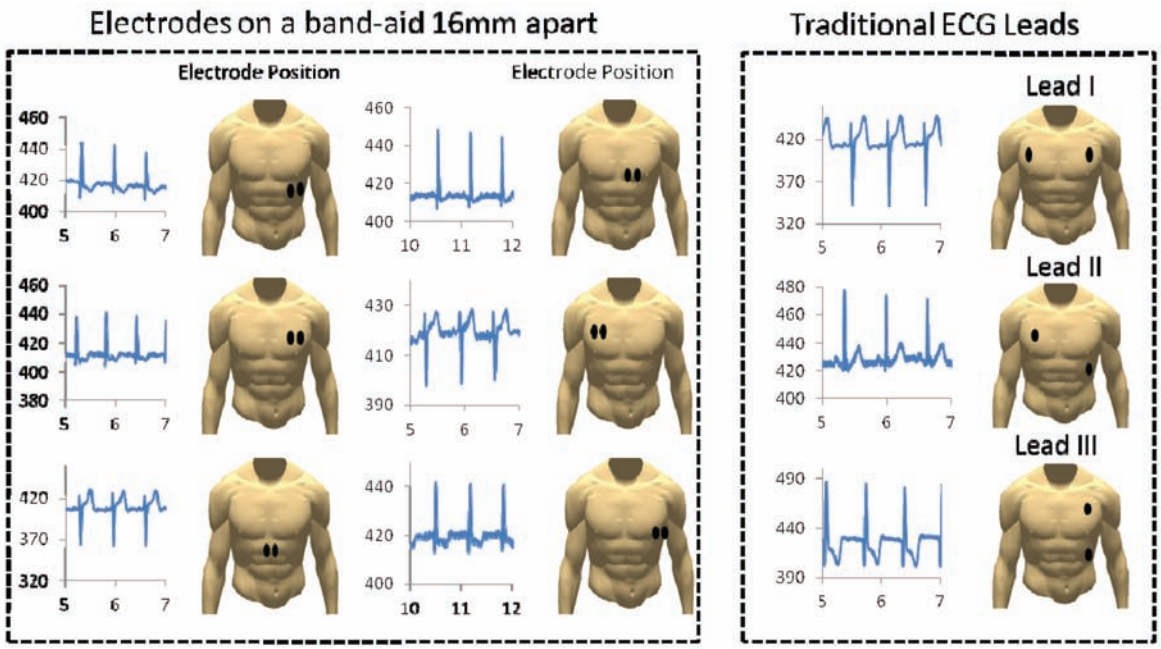

Figure 42 Different positions of band aid type e-Nanoflex and the ECG signal associated with it.

ratio. The three limb lead signals were obtained from commercial wet Ag/AgCl electrodes, *Moore Medical LLC.,* and from gold nanowire electrode as shown in Figure 41. The signals from the two electrodes are observably similar.

Band aid type e-Nanoflex can be placed at different positions relative to the heart to get different perspectives of the heart (Figure 42). Different positions enhance individual components of the ECG waveform, thus making each position relevant to the diagnosis of ECG abnormalities mentioned in the section on *Cardiological Signal Abnormalities*. The band aid sensor system can be potentially used for monitoring QT interval dispersion, which is prevalent in dialysis patients at risk of SCD. The system is simple to apply and does not interfere with the dialysis set up. Its adaptability to Bluetooth for a smartphone or PC makes it applicable in hospital dialysis as well as in POC for ambulatory dialysis.

The data from the e-Nanoflex sensors can also be sent to a remote server through the 3G

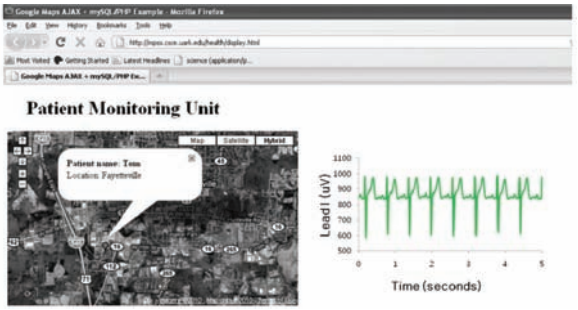

Figure 43 Snapshot of ECG data stored from the user and the corresponding location from where the data was sent.

network. The data were tagged with the current GPS location and the time. In the case of an emergency, a message with recorded data, current location and time can be sent to the emergency response team. The snapshot in Figure 43 shows the location of the user and also the data received from the sensor as recovered from the server.

6.2 e-Vests

The textile integrated sensor systems described in the previous sections are sensor elements that are inlaid between two layers of fabric or the fabric itself is functionalized to act as a sensor. The textile platform in this application is an inner vest that can incorporate nano-biosensors such as a gold nanowire electrode [Yoon *et al.*,2008] or a nanostructured textile electrode [Reneker *et al.*, 1996], or composite piezoelectric films [Laukhina *et al.*, 2010; Castellanos *et al.*, 2008]. It can also incorporate an infrared emitter-detection system for plethysmography and temperature sensors. The e-vest system is an implementation of a multichannel wearable wireless textile based nano-biosensor that monitors ECG and blood pressure.

System Description

Figure 44 shows the overall system which consists of four components. Firstly, a compression inner vest referred to as an e-vest, with textile electrode sensors and printed connection traces that connect the electrodes to a sensor electronics module (SEM). Secondly, there is a photoplethysmography arm band that has Near IR LEDs and photodiodes, which are connected to the SEM through conductive traces printed from the left arm. Thirdly, an SEM that consists of an amplifier and filter circuits, a microcontroller and a

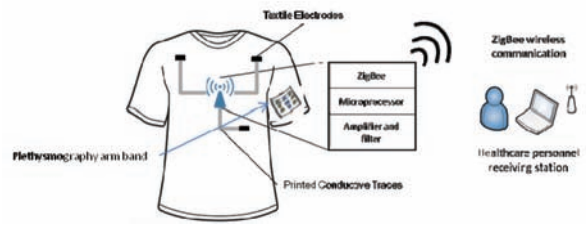

Figure 44 schematic showing overall system for acquisition of ECG through e-vest

ZigBee wireless radio module. Lastly, a software program runs on a PC, which receives and plots incoming data from the person wearing it.

The photoplethysmography arm band consists of two arrays of Near IR Photodiodes and a central array of three photodiodes. This assembly was described in detail in [Rai *et al.*, 2012]. The electrodes and the arm band are connected to the SEM through conductive traces printed on the vest. The conductive traces were made using conductive inks. The arm band is removable and simply snaps on to the vest through four snap buttons (Figure 45).

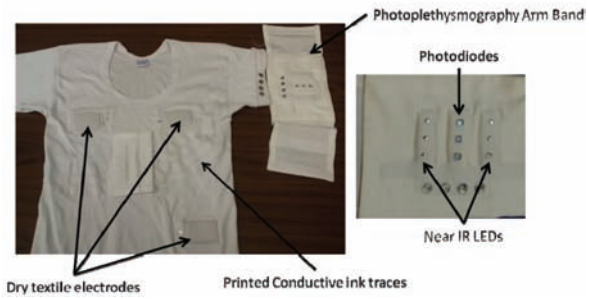

Figure 45 e-vest and the photoplethysmography arm band

The inks were formulated with conductive silver nanoparticle fillers in an elastic acrylic- based binder. The snap buttons were used for connections between the e-vest, the arm band, and the SEM after wearing the e-vest without any assistance. Screen printing, which is textile manufacturing compatible, was used to transfer the ink traces following the desired pattern for the conductive connecting traces. The removable SEM and arm band makes the e-vest washable.

Sensor Electronics Module (SEM)

The amplifier which is a part of the SEM consists of 4 channels. Three channels are for the bipolar limb leads- Lead I, Lead II and Lead III.

The fourth channel amplifies the potential difference across the photodiode which detects the reflected IR waves from the brachial artery. The amplifiers used in the SEM had a pass band of 0.2Hz to 70Hz and a mid- band gain of 50 dB for the three ECG channels. The gain was increased to 55dB for the photoplethysmography sensors for a band of 0.2Hz to 15Hz. The amplified signals from the amplifier are digitized using the onboard microcontroller for transmission (Figure 46).

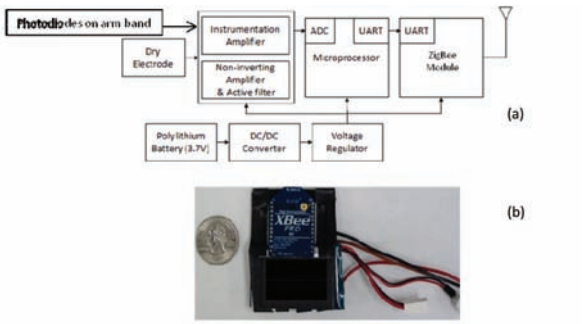

Figure 46 (a) Schematic of the SEM (b) actual SEM used in e-vest system.

The choice of a ZigBee radio module was motivated because of two desired functions. First, it has to support data rates higher than 9600 bps, because 4 channels of digitized ECG and BP signals have to be transmitted in real-time. Second, it provides communication ranges as high as possible for applications in sports, military expeditions and high risk work environments such as fire fighting (Figure 47).

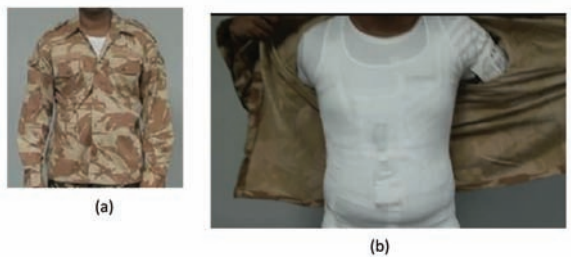

Figure 47 (a) subject wearing military fatigues (b) e-vest with arm band worn under the military fatigues.

6.3 e-Bras

The systems incorporated in the inner vests for men can also be integrated in inner garments for women such as a brassiere. The various sensors listed in the previous section can be incorporated in the e-bra and the signals from the sensors brought to the eNanoflex [Varadan *et al.*, 2011] module through printed conductive traces or conductive threads. Figure 48 shows a picture of the e-bra, the eNanoflex module used for data acquisition and wireless transmission, and the simple signal display interface that plots the data received from the eNanoflex module.

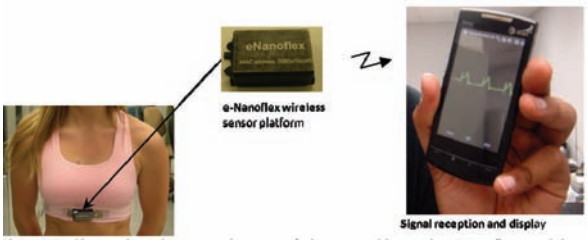

Figure 48 Shows the e-bra worn by one of the test subjects, the eNanoflex module and the Smartphone display interface

Multichannel data acquired

The data acquired by the e-vest can be transmitted wirelessly to a PC. The data received by the PC is then filtered using an adaptive filter algorithm to minimize the effect of motion on the ECG signal baseline [Kwon *et al.*, 2013]. The data acquisition and adaptive filter was developed using MATLAB (Mathworks, Natick, MA). However, the same can be achieved on a JAVA platform and can be deployed on a smartphone. Figure 49(a) shows the original 3 ECG signals Lead I, Lead II, and Lead III. It also plots the pulse waveform, the

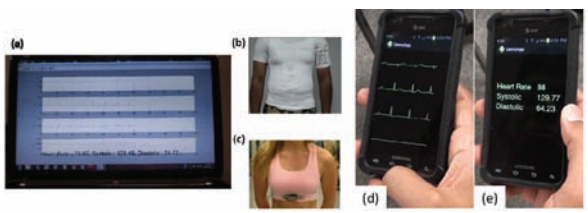

Figure 49 (a) Real-time data plotted on the laptop (b) the e-vest worn by the test subject (c) the e-bra worn by the test subject.

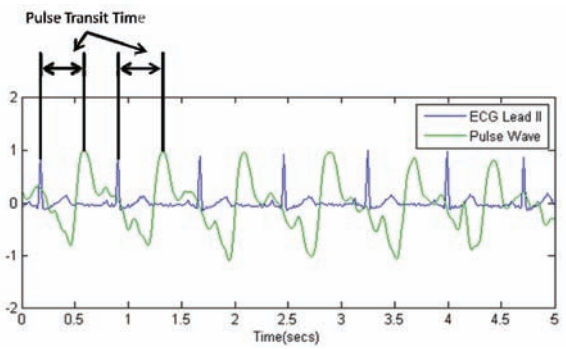

Figure 50 Simultaneous plot of ECG Lead II and Pulse wave depicting the derivation of PTT

heart rate, and the estimated systolic and diastolic blood pressure. 49 (b) shows the actual e-vest, arm band and SEM module. The derived pulse transit time PTT values (Figure 50) are then used to estimate the systolic and diastolic blood pressure values based on the calibration equations previously obtained in [Rai *et al.*, 2012]. Other sensor systems can be incorporated to develop wearable applications to monitor respiration, temperature and the blood oxygen level.

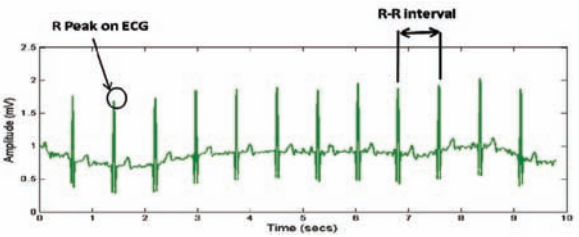

Figure 51 R-R interval calculations from ECG.

The Post processing of ECG can also calculate heart rate variability (HRV), which is a prognostic and diagnostic tool. HRV is described as the sequence formed by concatenating the difference in heart rate between consecutive beats (Figure 51). It is calculated as the inverse of the difference in the intervals between consecutive R-peaks. The R peak detection algorithm used for the calculation of the RR interval (RRI) was as given in [Pan *et al.*, 1985]. An Autoregressive (AR) power spectrum estimation technique was used to obtain the power spectrum density (PSD) plot of the RRI sequence. The characteristic LF and HF peaks were observed [Malik *et al.*, 1996]. Figure 52 shows a plot of the RR interval series plotted against beats and the AR PSD computed from the RRI series for the standing-up case. Figure 53 shows the same for supine ECG. AR PSDs in both figures show a classic shift in the power distribution between LF and HF components with respect to total power. Thus, these implementations of e-vest and e-bra systems can be used for the tracking of chronic conditions related to autonomous nervous regulation of cardiac activity.

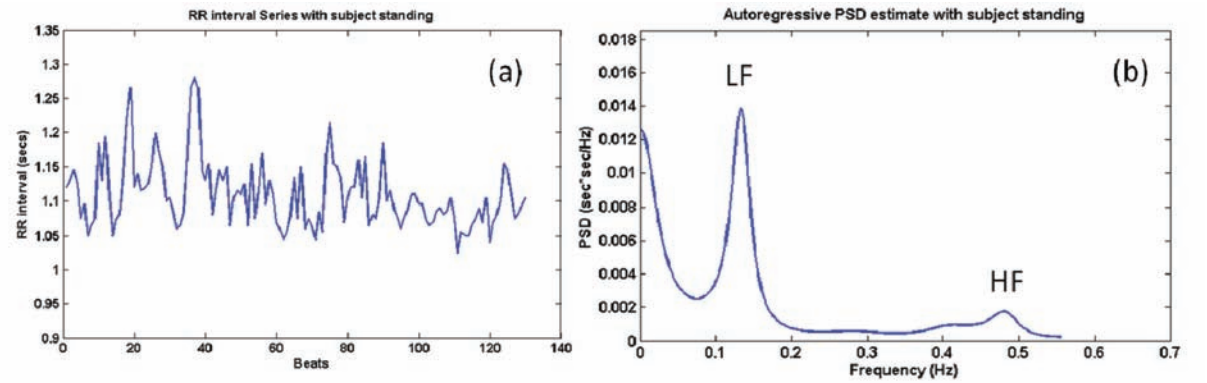

Figure 52 (a) Plot of the RR interval series against beat number (b) Plot of the AR PSD computed from the RRI series for the Standing case.

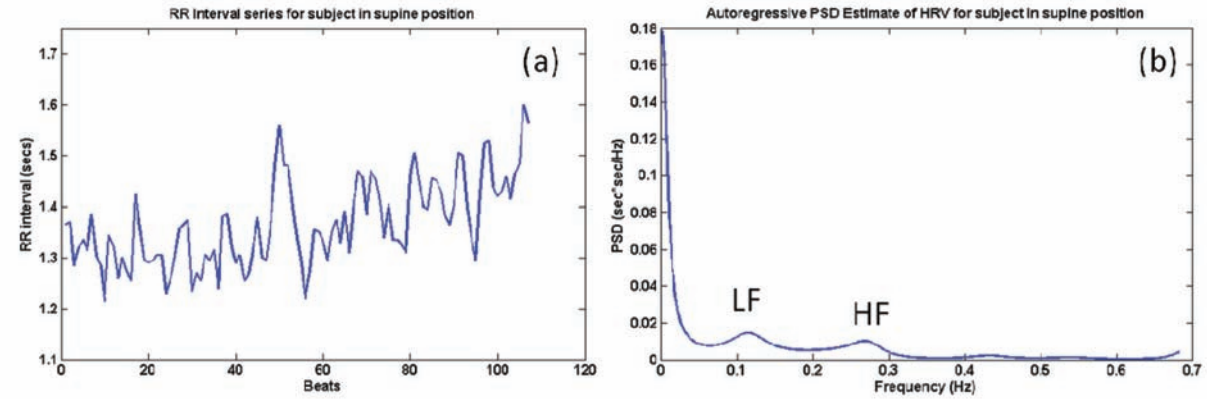

Figure 53 (a) Plot of the RR interval series against beat number (b) Plot of the AR PSD computed from the RRI series for supine position.

Continuous multiple lead ECG monitoring can be used for the detection of T-wave inversion, which is indicative of a change in ventricular repolarization as mentioned previously in the section on *Cardiological Signal Abnormalities*. The automated post processing of ECG by an algorithm for the detection of T wave inversion can serve as an alarm system that will trigger a subroutine to initiate ECG signal relay through a remote server to a doctor's office for a diagnosis.

7. Biofeedback System for Therapeutics

Since its introduction, smart wearable systems have been associated more with health monitoring than with therapeutics. These systems are, by nature, dependent on biometric inputs for analysis and response, and primarily inform of audio-visual cues and/or suggestions. So, while the systems described previously could only suggest medication or initiate medical intervention by doctors in remote locations, there have been proof-of-concept studies done to show that these systems can be of help in initiating audio-visual stimuli upon getting certain biosignals recorded by nanotextile biosensors. Such an automated system with a decision algorithm can be used to help control and/or cure the underlying medical condition. In this section, such systems have been described that can be used for therapeutics based on the biofeedback received by the sensors on board.

7.1 Music based Therapy

Music-based therapy has gained a lot of attention due to recent findings in the field of neuromusicology and music cognition. Music can evoke emotions through autonomic correlates that have been shown to cause a significant modulation of parameters like heart rate and blood pressure. Consequently, Heart Rate Variability (HRV) analysis can be a powerful tool to explore evidence-based therapeutic functions of music, and conduct empirical studies on the effect of musical emotion on heart function [Koelsch *et al.*, 2005; Khalfa *et al.*, 2002]. The HRV can be used to determine the autonomic nervous system activity. [Zhou *et al.*, 2010] Autonomic responses are known to vary according to the reports of valence (positive or negative) and arousal/intensity, which are considered as two dimensions of emotion [Lang *et al.*, 1998] including musical emotions [North *et al.*, 1997]. These emotions, in turn, have been shown to have strong autonomic correlates that regulate blood pressure and heart rate in the listener [Bernardi *et al.*, 2009]. Although the initial results are promising, much research is needed to understand the autonomic nervous system activity involved in musically induced emotions, the variations in brain processes with variations in the intensity and valence of the emotions experienced.

A Few studies have been performed to examine the brain process of emotions induced via an auditory domain stimulus like music. Figure 54 shows some preliminary EEG measurements after the application of an auditory stimulus in the form of happy and sad music. While listening to both

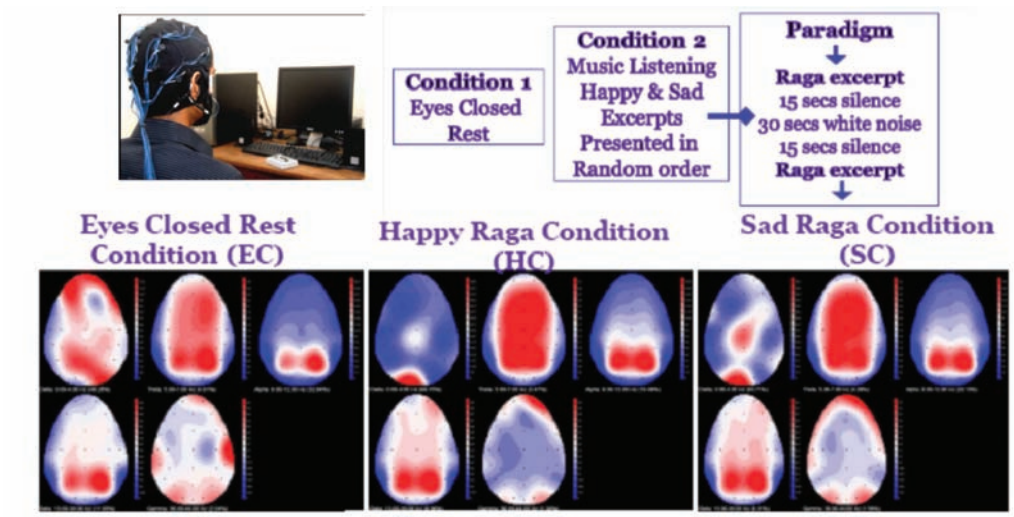

Figure 54 EEG measurements after application of auditory stimulus in the form of happy and sad music (Raga), with eyes closed rest condition as reference.

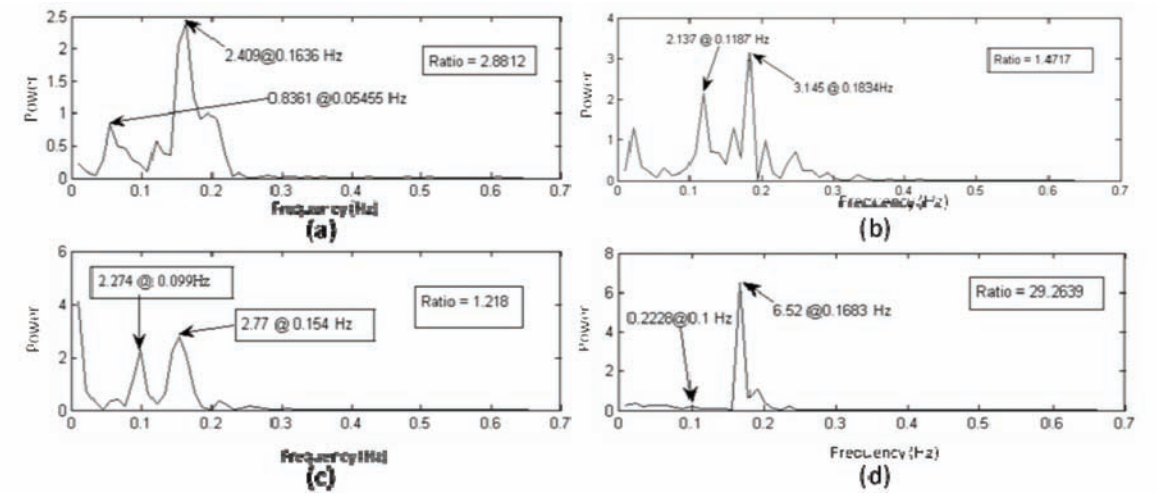

Figure 55 Shows the Periodogram of the HRV and High Frequency/Low Frequency power ration for ECG data for (a) No Music (b) Peppy (c) Happy (d) Sad Music

happy and sad music, there was an increase in Alpha wave power in the right hemisphere of the brain. There was also an increase in Delta, Theta and Gamma waves, but the extent of increase was greater during the happy music condition than in the sad music condition.

The textile- based nano-biosensor system for ECG monitoring, such as the e-vest and e-bra, can be used for recording ECG while listening to music. The plots in Figure 54 show the periodogram of the HRV signals for each type of music that was played during the recording. ECG data for two minutes, and one minute after the application of the stimulus music were used for a HRV analysis. The HRV analysis performed on this data shows that the emotion elicited by the type of music playing can modulate the autonomic regulation of the heart rate. A similar approach can be taken for EEG monitoring nanotextile biosensors. Music- based biofeedback therapy can be a potential treatment method to improve sensorimotor, language and cognitive domains of functioning via music. It can be especially helpful in invoking neuroplasticity for the rehabilitation of TBI patients. [Hegde, 2014]

7.2 Neural Activity based Biofeedback Therapy for Autism Spectrum Disorder

Autism Spectrum Disorder (ASD) covers neurological disorders that involve impeded development of social behavior, and the acquisition of skills and language development. All these activities require the ability of mimicry by which children imitate and learn the appropriate forms of the aforementioned attributes. The ability to mimic is associated with a class of neurons called the mirror neurons found in the insula and anterior cingulate cortex of the brain, which are responsible for the interpretation of complex human intentions. The functioning of these neurons can be observed by monitoring Mu waves in those regions using EEG. Mu waves are synchronized patterns of electrical activity involving large numbers of neurons in the part of the brain that controls voluntary functions. In normal subjects, the Mu waves are suppressed when the voluntary function has been executed, whereas in ASD subjects, the suppression does not happen because no function was executed.

Conventional EEG measurement systems use gel based gold cup electrodes, attached to the scalp with adhesive. It is obtrusive and the wires sticking out of the electrodes to signal acquisition systems make them impractical for use in sensitive subjects like infants and children with ASD. Alternatively, nanotextile biosensors can be incorporated with a skull cap and baseball cap that are commonly used for infants and children. Textile based multi-electrode EEG, EOG and EMG monitoring systems with embedded electronics for data acquisition and wireless transmission can be seamlessly integrated into these items for the continuous detection of Mu waves (Figure 55). Textile electrodes at positions C3, CZ, C4 according to the 10-20 international system can detect Mu waves. The textile- based system is ergonomic and can enable early diagnosis

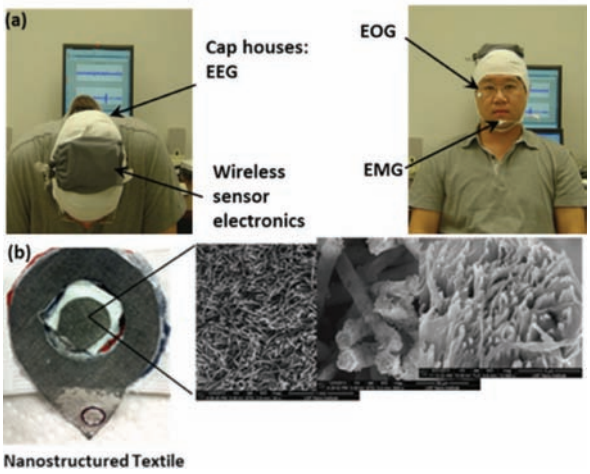

Figure 55 EEG, EOG and EMG are acquired on the skin through conductive textile electrodes. The acquisition of EEG through the hair on the head was made possible by using nano- structured conductive electrode with long pillars of conductive textile to serve this purpose.

in infants and planning therapy for ASD patients. [Sahi *et al.*, 2013]

Biofeedback can be used for therapeutic purposes for Autism Spectrum Disorder (ASD) by operant conditioning. By giving stimuli in the form of repetitive audio/visual cues to emulate a voluntary function (waving hand, saying hello, and open –close fist) and monitoring the change in Mu wave intensity, the system can condition the subject. The audio-visual loop can be controlled by the embedded logic that breaks the loop only upon detecting Mu wave occurrence and suppression, after which it will choose another cue from the audio-visual library on the system. This system can help in ASD diagnostics by monitoring Mu waves for detecting anomalies in the brain wave patterns of mirror neurons [Ramachandran *et al.*, 2006]. The automated system can be used at home under parental guidance, while keeping the therapist updated at remote locations through the internet

8. Conclusions

Wearable textile- based nano-biosensor systems with mobile platforms are a new class of unobtrusive continuous health monitoring with significant benefits for neurological and cardiovascular patients or high risk patients. The basic science behind the functioning of textile- based nano-biosensors show that there is a better flow of signal i.e. electrical current through the skin-electrode interface than through the silver-silver chloride gel electrode. The bioelectromagnetic principles of the origin and propagation of bioelectric signals i.e. EEG, EOG, EMG and ECG show that the measured electric potential is representative of the cumulative electrical activity of the sources of these signals, i.e. the neurons of brain tissue and the myocytes of heart tissue. This means that the textile- based nano-biosensors can measure bioelectric signals better than the silver-silver chloride gel electrode. The dry electrodes can be used for long term monitoring because they do not face the problem of the drying of the gel and they are reusable in the form of a wearable garment. The textile- based wearable nano-biosensor systems discussed in this review can measure neurological signals and identify anomalies for the diagnosis of targeted neurological and cardiovascular disorders. These disorders range from chronic conditions to safety to rehabilitation and an improved quality of life. The bioelectromagnetism principles of neural and cardiac bioelectric signals and the performance of textile-based nano-biosensors provides a unique perspective on the development of novel wearable systems that harness the potential of textile based nano-biosensors and wireless platforms for understanding the neural and cardiac function in and out of hospital setting in unprecedented detail. The sensor systems can be used for the diagnostics and therapeutics of neurological disorders such as autistic spectrum disorder, traumatic brain injury (TBI), and neuroprosthetics. They can be used for highly specialized cardiac monitoring such as vector cardiography (VCG), impedance cardiography (ICG) or tomography, tumor detection, and the prevention of sudden cardiac death by the detection of T-wave alternans.

Acknowledgments

One of the authors, Vijay K. Varadan would like to extend his gratitude to 289 Dr. Vasudev K. Aatre for his constant and continuing support, encouragement, and mentorship 290 during the course of his research work in acoustics, electromagnetics, smart materials and sys- 291 tems, and health care. This research was conducted with the endowment for smart textiles for 292 health care, from Global Institute for Nanotechnology in Engineering and Medicine Inc., 700 293 Research Center Blvd., Fayetteville, AR 72701.

References:

Aarts, E., Marzano, S., "The New Everyday-Visions on Ambient Intelligence," 101 Publishers, Rotterdam, The Netherlands. (2003)

Alzadi, A., Zhang, L., Bajwa, H., "Smart Textile Based Wireless ECG System," Proc. IEEE Systems, Applications and Technology Conference (LISAT) 2012, pp. 1-5. (2012)

Baker, W.R., "Microdenier spinning," Int. Fiber J., April 1992, pp. 7-15. (1992)

Barhate, R.S., Ramakrishna, S., "Nanofibrous filtering media: Filtration problems and solutions from tiny materials," J. Membrane Science, Vol. 296, pp. 1-8. (2007)

Bashashati. A, Fatourechi. M, Ward. R.K, Birch. G.E, "A survey of signal processing algorithms in brain-computer interfaces based on electrical brain signals," J. Neural Eng., vol. 4, pp. 32-57, 2007.

Bergey, G.E., Squires, R.D., Sipple, W.C., "Electrocardiogram Recording with Pasteless Electrodes," IEEE Transactions on Bio-medical Engineering, Vol, BME-18 (3), pp. 206-211. (1971)

Bernardi. L, Porta. C, Casucci. G, Balsamo. R, Bernardi. N.F, Fogari. R, Sleight. P, "Dynamic Interactions Between Musical, Cardiovascular, and Cerebral Rhythms in Humans.", Circulation,119,3171-3180(2009).

Brevnov, D.A., "Electrodeposition of Porous Silver Films on Blanket and Patterned Aluminum-Copper Films," L. Electrochem. Soc., Vol. 153 (4), pp. C249-C253. (2006)

Brosche, T.A.M., "EKG Handbook," Jones and Bartlett, Sudbury, M.A., Section 10, pp.87-98. (2010)

Castellanos, J; Navas-Gonzalez, R; Ochoteco, E; Vidal-Verdu, F; , "Evaluation of a low cost piezorresistive material for high resolution tactile sensors," Integration Issues of Miniaturized Systems - MOMS, MOEMS, ICS and Electronic Components (SSI), 2008 2nd European Conference & Exhibition on , vol., no., pp.1-3, 9-10 April 2008.

Catanzaro JN, Meraj PM, Zheng S, Bloom G, Roethel M, Makaryus AN.,"Electrocardiographic T-wave changes underlying acute cardiac and cerebral events.", Am J Emerg Med. 2008 Jul;26(6):716-20.

Catrysse, M., "Wireless power and data transmission for implantable and wearable monitoing systems," PhD Thesis, K. U. Leuven. (2004)

CDC, "10 Leading Causes of Death by Age Group, United States 2005-2010," National Vital Statistics System, National Centre for Health Statistics, Centres for Disease Control (CDC). (2005-2010)

CDC, National Center for Chronic Disease Prevention and Health Promotion, "Chronic Disease Prevention and Health Promotion," http://www.cdc.gov/chronicdisease/index.htm (2013)

Chapin. J, Moxon. K, Markowitz. R, Nicolelis. M, "Real-time control of a robot arm using simultaneously recorded neurons in the motor cortex," Nature Neurosci., vol. 2, pp. 664–670, 1999.

Chow T, Kereiakes DJ, Bartone C, Booth T, Schloss EJ, Waller T, Chung ES, Menon S, Nallamothu BK, Chan PS. "Prognostic utility of microvolt T-wave alternans in risk stratification of patients with ischemic cardiomyopathy.", J Am Coll Cardiol. 2006 May 2;47(9):1820-7.

Clemens, F., *et al*., "Computing Fibers: A Novel Fiber for Intelligent Fabrics?" Advanced Engineering Materials, Vol. 5 (9), pp. 692-687. (2003)

Coosemans, J., Hermans, B., Peurs, R., "Integrating wireless ECG in textiles," Sensors and Actuators A, 130-131, 48-53 (2006).

Cox V, Patel M, Kim J, Liu T, Sivaraman G, Narayan SM.,"Predicting arrhythmia-free survival using spectral and modified-moving average analyses of T-wave alternans.", Pacing Clin Electrophysiol. 2007 Mar;30(3):352-8.

D. Marculescu, R. Marculescu, N.H. Zamora, P.S. Marbell, P.K. Khosla, S. Park, S. Jayaraman, S. Jung, C. Lauterbach, W. Weber, T. Kirstein, D. Cottet, J. Grzyb, G. Troster, M. Jones, T. Martin, Z. Nakad, "Electronic Textile: A Platform for Pervasive Computing," Proc. of IEEE, Vol. 91 (12), pp.1995-2018. (2003)

David, R.M., Portnoy, W.M., "Insulated Electrocardiogram Electrodes," Med. &Biol. Eng., Vol. 10, pp. 742-751. (1972)

de la Maisonneuve, C., Martins, J.O., "Public spending on health and long-term care: a new set of projections," OECD Economic Policy Papers, no. 6. (2013) http://www.oecd.org/economy/public-

spending-on-health-and-long-term-care.htm

De Rossi, D., Carpi, F., Lorussi, F., Mazzoldi, A., Paradiso, R., Scilingo, E.P., Tognetti, A., "Electroactive Fabrics and Washable Biomonitoring Devices," AUTEX Research Journal, Vol. 3(4), pp. 180-185. (2003)

Dhawan, A., Muth, J., F., Kekas, D., J., Ghosh, T., K., "Optical nano-textile sensors based on the incorporation of semiconducting and metallic nanoparticles into optical fibers," Smart Nanotextiles. Symposium (Materials Research Society Symposium Proceedings, 920, 121-126. (2006)

Eckart RE, Scoville SL, Campbell CL, Shry EA, Stajduhar KC, Potter RN, Pearse LA, Virmani R., "Sudden death in young adults: a 25-year review of autopsies in military recruits.", Ann Intern Med. 2004 Dec 7;141(11):829-34.

European Transport Safety Council, "The Role of Driver Fatigue in Commercial Road Transport Crashes", 2001

Fine, E.J., Ionita, C.C., Lohr, L., "The history of the development of the cerebellar examination," Seminars in Neurology, Vol. 22 (4), pp. 375-384. (2002)

Flemons. W, Douglas. J, Kuna. T, Rodenstein. O, Wheatley. J, "Access to diagnosis and treatment of patients with suspected sleep apnea," American Journal of Respiratory Care Medicine, vol. 169(2), pp. 668-672, 2004.

Garcia, T.B., Holtz, N.E., "12-lead ECG: The art of interpretation," Jones and Bartlett, Sudbury, M.A. (2001)

Gehi AK, Stein RH, Metz LD, Gomes J. "Microvolt T-Wave Alternans for the Risk Stratification of Ventricular Tachyarrhythmic Events: A Meta-Analysis." J Am Coll Cardiol. 2005;46(1):75-82.

Geselowitz D.B. "Dipole theory in Electrocardiography.", Am. J . Cardiol. 1964 Sep; 14:301-6. (1964)

Gimpel, S., et.al., "Textile-based Electronics Substrate Technology," Journal of Industrial Textiles, Vol. 33(3), pp. 179-189. (2004)

Go A.S, Mozaffarian D, Roger VL, Benjamin EJ, Berry JD, Borden WB, Bravata DM, Dai S, Ford ES, Fox CS, Franco S, Fullerton HJ, Gillespie C, Hailpern SM, Heit JA, Howard VJ, Huffman MD, Kissela BM, Kittner SJ, Lackland DT, Lichtman JH, Lisabeth LD, Magid D, Marcus GM, Marelli A, Matchar DB, McGuire DK, Mohler ER, Moy CS, Mussolino ME, Nichol G, Paynter NP, Schreiner PJ, Sorlie PD, Stein J, Turan TN, Virani SS, Wong ND, Woo D, Turner MB; American Heart Association Statistics Committee and Stroke Statistics Subcommittee."Heart disease and stroke statistics—2013 update: a report from the American Heart Association.",Circulation. 2013 Jan 1;127(1):e6-e245.

Gray, H., "Anatomy of the Human Body," 40th Ed., Churchill Livingstone, Elsevier. (2008) ISBN 978-0-443-06684-9

H. Jorg, "My Heart," European Community 6th Framework Programme, 2003-2008. www.cordis.europa.eu

Hegde, S., "Music based cognitive remediation therapy for patients with traumatic brain injury," Frontiers in Neurology, Vol. 5 (34), (2014)

Herzog CA, Mangrum JM, Passman R.,"Sudden cardiac death and dialysis patients", Semin Dial. 2008 Jul-Aug;21(4):300-7.

Holder D.S, "Electrical Impedance Tomography: Methods, History and Applications,", Institute of Physics, Series in medical Physics and Biomedical Engineering, London. (2005)

Holme, I., "Nanotechnologies for Textiles, Clothing, and Footwear," Textile Magazine, Vol. 32 (1), pp. 7-11. (2005)

Huang. J; Wang. L; Chen. L; Zhang YT; , "A low power wearable transceiver for human body communication," Engineering in Medicine and Biology Society, 2009. EMBC 2009. Annual International Conference of the IEEE , vol., no., pp.3802-3805, 3-6 Sept. 2009.

Iber, S. Ancoli-Israel, A. Chesson, S. Quan, "The AASM Manual for the Scoring of Sleep and Associated Events: Rules, Terminology, and Technical Specifications," Amer. Acad. Sleep Med, Westchester, IL, 2007.

Jahrsdeorfer, M., Guiliano, K., Stephens, D., "Clinical usefulness of the EASI 12-lead continuous electrocardiographic monitoring system," Critical Care Nurse, Vol. 25(5), pp. 28-37. (2005)

Jap BT, Lal. S, Fischer. P, Bekiaris. E, "Using EEG spectral components to assess algorithms for detecting fatigue", Expert Systems with Applications Vol.36

Issue 2, pp. 2352-2359, 2009

Jiang, S.Q., Newton, E., Yuen, C.W.M., Kan, C.W., "Chemical Silver Plating on Cotton and Polyester Fabrics and its Application on Fabric Design," Textile Research Journal, Vol. 76 (1), pp. 57-65. (2006)

Kandel E.R., Schwartz, J.H., Jessel, T.M., "Principles of Neural Science," McGraw-Hill Professional, pp. 324. (2000)

Khalfa, S., Isabelle, P., Jean-Pierre, B., Manon, R. "Event-related skin conductance responses to musical emotions in humans." Neurosci Lett, 328(2), 145-149(2002).

Khan. G. M, "Rapid ECG Interpretation", Humana Press; 3rd edition (2007), p25-297.

Khosla, A., "Smart garments in chronic disease management: progress and challenges," Proc. SPIE Vol. 8548, Nanosystems in Engineering and Medicine, 85482O. (2012)

Klingenheben T, Zabel M, D'Agostino RB, Cohen RJ, Hohnloser SH."Predictive value of T-wave alternans for arrhythmic events in patients with congestive heart failure.",Lancet. 2000 Aug 19;356(9230):651-2.

Koelsch, S., Siebel, W. A., "Towards a neural basis of music perception." Trends Cogn Sci, 9(12), 578-584(2005).

Kwon, H., Oh, S., Varadan, V.K., "Motion artifact removal algorithm by ICA for e-bra: a women ECG measurement system," Proc. SPIE 8691, Nano- Bio- and Info_tech Sensors and Systems 2013, 86910A. (2013)

Lang, P. J., Bradley, M. M., Cuthbert, B. N., "Emotion and motivation: measuring affective perception." J Clin Neurophysiol, 15(5), 397-408(1998).

Laukhina, E.; Pfattner, R.; Mas-Torrent, M.; Rovira, C.; Veciana, J.; Laukhin, V.; , "Flexible Film-Based Sensors Structured with a High Piezoresistive Organic Molecular Conductor as an Active Component," Sensor Device Technologies and Applications (SENSORDEVICES), 2010 First International Conference on , vol., no., pp.4-9, 18-25 July 2010

Led, S., Martinez-Espronceda, M., Redondo, J., Baquero, A., Serrano, L., Cabezas, L., Niegowski, M., "Wearable electrocardiogram (ECG) recorder for a Mobile Point-of-Care based on recent interoperability standards," Point-of-Care Healthcare Technologies (PHT), 2013 IEEE , pp.287-290. (2013)

Lee RG; Chen KC; Hsiao CC; Tseng CL; , "A Mobile Care System With Alert Mechanism," Information Technology in Biomedicine, IEEE Transactions on , vol.11, no.5, pp.507-517, Sept. 2007

Lee, Y., D., Chung, W., Y., "Wireless sensor network based wearable smart shirt for ubiquitous health and activity monitoring," Sensors and Actuators B, 140, 390-395 (2009).

Lim, Z., H., Chia, Z., X., Kevin, M., Wong, A., S., W., Ho, G., W., "A facile approach towards ZnO nanorods conductive textile for room temperature multifunctional sensors," Sensors and Actuators B: Chemical, 151 (1), 121-126. (2010)

Lin CT; Wu RC, "EEG-based drowsiness estimation for safety driving using independent component analysis", Circuits and Systems I: Regular Papers, Vol. 52, Issue 12, pp. 2726 - 2738, Dec. 2005

Locher, I., Klemm, M., Kirstein, T., Troster, G., "Design and Characterization of Purely Textile Patch Antennas," Vol. 29 (4), pp. 777-788. (2006)

M. Ramasamy, S. Oh, V. K. Varadan and Robert Harbaugh2,3 "Textile based Nanosensors and Wireless Mobile Communication Platform for Real Time Driver Alertness Monitoring" Smart Nanosystems in Engineering and Medicine Vol 2, Issue 2, May, 2013.

Maeda S, Nishizaki M, Yamawake N, Ashikaga T, Shimada H, Asano M, Ihara K, Murai T, Suzuki H, Fujii H, Sakurada H, Hiraoka M, Isobe M."Ambulatory ECG-based T-wave alternans and heart rate turbulence predict high risk of arrhythmic events in patients with old myocardial infarction.",Circ J. 2009 Dec;73(12):2223-8.

Maharani, D., K., Kartini, I., Aprilita, N., H., "Nanosilica-Chitosan Composite Coating on Cotton Fabrics," Third Nanoscience and Nanotechnology Symposium 2010, 1284, 87-91. (2010)

Malik. M, Bigger. J.B, Camm. A.J, Kleiger.R.E, Malliani. A, Moss.A.J, Schwartz.P.J,"Heart rate variability: Standards of measurement, physiological interpretation, and clinical use" Eur Heart J (1996) 17 (3): 354-381

Malmivuo, J., Plonsey, R., "Bioelectromagnetism: Principles and Applications of Bioelectric and Biomagnetic Fields," Chapter 2, Oxford University Press, New York. (1995) ISBN 0-19-505823-2

Mazzoldi, A., De Rossi, D., Lorussi, F., Scilingo, E.P., and Paradiso, R., "Smart Textiles for Washable Motion Capture Systems," AUTEX Research Journal, Vol. 2(4), pp. 199-203. (2002)

Merchant FM, Ikeda T, Pedretti RF, Salerno-Uriarte JA, Chow T, Chan PS, Bartone C, Hohnloser SH, Cohen RJ, Armoundas AA."Clinical utility of microvolt T-wave alternans testing in identifying patients at high or low risk of sudden cardiac death." Heart Rhythm. 2012 Aug;9(8):1256-64.e2.

Munirathinam, V., Anandhan, G., Paramasivam, M., "Enhanced sensing of anthraquinone dye using multiwalled carbon nanotubes modified electrode," Int. J. Environmental Analytical Chem., Vol. 93 (3), pp. 349-363. (2013)

Naik, A., "Future impact of nanotechnology in textile research," Proc. II Int. Symposium in Textile Engineering Natal Brazil, pp. 7-11. (2004)

Neale, V. L., Dingus, T. A., Klauer, S.G., Sudweeks, J., Goodman, M., "An Overview of the 100-Car Naturalistic Study and Findings," ESV Paper 05-0400, June 2005.

Nicolelis. M, "Brain-machine interfaces to restore motor function and probe neural circuits," Nature Rev. Neurosci., vol. 4, pp. 417–422, 2003.

Niedermeyer E., da Silva F.L. (2004). Electroencephalography: Basic Principles, Clinical Applications, and Related Fields. Lippincot Williams & Wilkins. ISBN 0-7817-5126-8

Nilson. T, Nelson T.M, Carlson D., "Development of Fatigue Symptoms During Simulated Driving", Accidents Analysis &Prevention Vol. 29, No 4. pp. 479-488.1997

North, A. C., Hargreaves, D. J., "Liking, arousal potential, and the emotions expressed by music." Scand J Psychol, 38(1), 45-53(1997).

Noueihed. J, Diemer. R, Chakraborty. S, Biala. S, "Comparing Bluetooth HDP and SPP for Mobile Health Devices," Body Sensor Networks (BSN), 2010 International Conference on , vol., no., pp.222-227, 7-9 June 2010

Numetrex® Heart Monitoring Apparel. www.numetrex.com

Oh, T.I., Yoon, S., Kim, T.E., Wi, H., Kim, K.J., Woo, E.J., Sadleir, R.J., "Nanofiber Web Textile Dry Electrodes for Long-Term Biopotential Recording," IEEE Trans. Biomedical, Circuits and Systems, Vol. 7(2), pp. 204-211. (2013)

Oh. S, Kumar. P.S, Kwon. H, Varadan.V.K, "Wireless brain-machine interface using EEG and EOG: brain wave classification and robot control," SPIE Proceedings, vol. 8344, 2012.

Pacelli, M., Caldani, L., Paradiso, R., "Textile Piezoresistive Sensors for Biomechanical Variables Monitoring," Proc. 28th Ann. Int. Conf. IEEE EMBS 2006, pp. 5358-5361. (2006)

Pan, J; Tompkins, W.J.; "A Real-Time QRS Detection Algorithm," Biomedical Engineering, IEEE Transactions on , 32(3), 230-236 (1985).

Pantelopoulos, A., Bourbakis, N., "A survey on wearable biosensor systems for health monitoring,"30th Annual Int. Conf. of the IEEE, EMBS 2008, pp. 4887-4890. (2008)

Pantelopoulos. A, Bourbakis N. G., "A Survey on Wearable Sensor-Based Systems for Health Monitoring and Prognosis.", IEEE Transactions on Systems Man and Cybernetics—part c: applications and reviews, 40(1), (2010)

Park, S, Gopalsamy, C., Rajamanickam, R., Jayaraman, S., "The Wearable MotherboardTM : An Information Infrastructure or Sensate Liner for Medical Applications," Studies in Health Technology and Informatics, IOS Press, Vol. 62, pp. 252-258. (1999)

Park, S., Jayaraman, S., "Wearable Biomedical Systems: Research to Reality," Proc. IEEE Int. Conf. Portable Information Devices PORTABLE07, pp. 1-7. (2007)

Pejis, T., Chairman Smart Textiles Symposium (in call for papers), Plastic Electronics Conference, September 2005, Frankfurt, www.plastictronics.org. (2005)

Post, E.R, Orth, M., "Smart Fabric, or Washable Computing," Proc. IEEE Int. Symposium on Wearable Computers, Cambridge (MA), USA, Oct. 1997, pp. 167-168. (1997)

Pun PH, Horton JR, Middleton JP.,"Dialysate calcium concentration and the risk of sudden cardiac arrest in hemodialysis patients.", Clin J Am Soc Nephrol. 2013 May;8(5):797-803.

Rai, P., "Hybrid Nanostructured Textile Bioelectrode for unobtrusive health monitoring," Doctoral Dissertation, University of Arkansas, ProQuest , UMI Dissertations Publishing, ISBN 9781303276231. (2013)

Rai, P., Kumar, P.S., Oh, S., Kwon, H., Mathur, G.N.,

Varadan, V.K., Agarwal, M.P., "Smart healthcare textile sensor system for unhindered-pervasive health monitoring," SPIE Smart Structures+NDE, Nano., Bio. & Info-Tech. Sensors and Systems 2012, Vol. 8344, 83440E. (2012)

Ramachandran, V.S., Oberman, L.M., "Broken Mirrors A Theory of Autism," Scientific American, November 2006, pp. 63-69. (2006)

Ranney, T. et al. "NHTSA Driver Distraction Research: Past, Present and Future", Driver Distraction Internet Forum, 2000.

Rattfalt, L.; Chedid, M.; Hult, P.; Linden, M.; Ask, P., "Electrical Properties of Textile Electrodes," Engineering in Medicine and Biology Society, 2007. EMBS 2007. 29th Annual International Conference of the IEEE , vol., no., pp.5735-5738, 22-26 Aug. 2007

Rawles, J., "Magnitude of benefit from earlier thrombolytic treatment in acute myocardial infarction: new evidence from Grampian region early anistreplase trial (GREAT)," BMJ, Vol. 312, pp. 212-215. (1996)

Reisner A. T, Clifford G. D, Mark.R.G, Course materials for HST.582J / 6.555J / 16.456J,Biomedical Signal and Image Processing, Spring2007. MIT OpenCourseWare (http://ocw.mit.edu), Massachusetts Institute of Technology.

Reneker, D.H., Chun, I., "Nanometer diameter fibers of polymer, produced by electrospining," Nanotechnology, Vol. 7, pp. 216-223. (1996)

Ribeiro AL, Rocha MO, Terranova P, Cesarano M, Nunes MD, Lombardi F.,"T-wave amplitude variability and the risk of death in Chagas disease.", J Cardiovasc Electrophysiol. 2011 Jul;22(7):799-805.

Rita Levi-Montalcini, "Neurological disorders – Public health challenges" 2007

Robertson. G, Caldwell. G, Hamill. J, Kamen. G, Whittlesey. S, "Research Methods in Biomechanics.", Chapter 8, p171-181 Champaign, IL: Human Kinetics Publ., 2004.

Sahi, A., Rai, P., Oh, S., Ramasamy, M., Harbaugh, R.E., Varadan, V.K., "Neural Activity based Biofeedback Therapy for Autism Spectrum Disorder through Wearable Wireless Textile EEG Monitoring System," Proc. SPIE 8691, Nano- Bio- and Info_tech Sensors and Systems 2013, 86910A. (2013)

Sahoo, S., Ouyang, H., Goh, J.C.H., Tay, T.E., Toh, S.L., "Characterization of a novel polymeric scaffold application in tendon/ligament tissue engineering," Tissue Engineering, Vol. 12, pp. 91-99. (2006)

Saroj K.L. Lal, Ashley Craig, "A critical review of the psychophysiology of driver fatigue", Biological Psychology, Volume 55, Issue 3, 1 February 2001, p173-194.

Serruya. M, Hatsopoulos. N, Paninski. L, Fellows. M, Donoghue. J, "Instant neural control of a movement signal," Nature, vol. 416, pp. 141–142, 2002.

Shen. J, Barbera. J, Shapiro. C.M, Distinguishing sleepiness and fatigue: focus on definition and measurement, Sleep Medicine Reviews, Volume 10, Issue 1, February 2006, p 63-76.

Shyamkumar. P, Oh. S, Banerjee. N, Varadan. V.K., " A Wearable Remote Brain Machine Interface using Smartphones and the Mobile Network," Proceedings of Advances in Science and Technology, vol. 85, pp. 11-16, 2012. Smart T-shirt by GOW Trainer. www.gowtrainer.com

Tao, X., "Smart Fibers, Fabrics and Clothing," Cambridge, Woodhead. (2001)

Taylor. D, Tillery. S, Schwartz. A, "Direct cortical control of 3D neuroprosthetic devices," Science, vol. 296, pp. 1829–1832, 2002.

Tonezzer, M., Lacerda, R.G., "Zinc oxide on carbon microfiber as flexible gas sensor," Physica E: Low-dimensional Systems and Nanostructures, Vol. 44 (6), pp. 1098-1102. (2012)

Varadan, V., K., Kumar, P., S., Oh, S., Kwon, H., Rai, P., Banerjee, N., and Harbaugh R., E., "e-Nanoflex Sensor Systems: Smartphone-Based Roaming Health Monitor," L. Nanotechnol. Eng. Med., 2 (1), 011016 (11 pages). (2011)

Varadan, V., K., Oh, S., Kwon, H., and Hankins, P., "Wireless Point-of-Care Diagnosis for Sleep Disorder With Dry Nanowire Electrodes," J. Nanotechnol. Eng. Med., 1 (3), 031012 (11 pages). (2010)

Vigneshwaran N., Kumar, S., Kathe, A., A., Varadarajan, P., V., Prasad, V., "Functional finishing of cotton fabric using zinc oxide-soluble starch nanocomposites," Nanotechnology, 17 (20), 5087-5095. (2006)

Wang, H., Wang, J, Hong, J., Wei, Q., Gao, W, Zhu, Z., "Preparation and characterization of silver nanocomposite textile," J. Coat. Technol. Res., Vol. 4 (1), pp. 101-106. (2007)

Wearable Wellness System from Smartex s.r.l. Pisa Italy. www.smartex.it

Wearable Wellness System from Smartex s.r.l. Pissa Italy. www.smartex.it

Wessberg. J, Stambaugh. C, Kralik. J, Beck. P, Laubach.

M, Chapin. J, Kim. J, Biggs. S, Srinivassan. M, Nicolelis. M, "Real-time prediction of hand trajectory by ensembles of cortical neurons in primates," Nature, vol. 408, pp. 361-365, 2000.

Wilson, M.G., Sharma, S., Carre, F., Charron, P., Richard, P., Hanlon, R.O., Prasad, S.K., Heidbuchel, H., Brugada, J., Salah, O., Sheppard, M., George, K.P., Whyte, G., Hamilton, B., Chalabi, H., "Significance of deep T-wave inversions in asymptomatic athletes with normal cardiovascular examinations: practical solutions for managing the diagnostic conundrum," British Journal of Sports Medicine, Vol. 46 (Suppl. I), pp. i51-i58. (2012)

Wolpaw. J, Birbaumer. N, McFarland. D, Pfurtscheller. G, Vaughan. T, "Brain-computer interfaces for communication and control," Clin. Neurophysiol., vol. 113, pp. 767-791, 2002.

Wolpaw. J, Birbaumer. N, McFarland. D, Pfurtscheller. G, Vaughan. T, "Brain-computer interfaces for communication and control," Clin. Neurophysiol., vol. 113, pp. 767-791, 2002.

Wu VC, Lin LY, Wu KD., "QT interval dispersion in dialysis patients", Nephrology (Carlton). 2005 Apr;10(2):109-12.

Xue, P., Tao, X.M., "Morphological and Electromechanical Studies of Fibers Coated with Electrically Conductive Polymer," Vol. 98 (4), pp. 1844-1854. (2005)

Yeon, S.J., "Study on texture evolution and properties of silver thin film prepared by sputtering deposition," Appl. Surf. Sci., Vol. 221, pp. 281-287. (2004)

Yoon, H., Deshpande, D.C., Ramachandran, V., Varadan V.K., "Aligned nanowires growth using lithography-assisted bonding of a polycarbonate template for neural probe electrodes," Nanotechnology, Vol. 19, 025304 (8pp). (2008)

Young. T, Palta. M, Dempsey. J, Skatrud. J, Weber. S, Badr. S, "The occurrence of sleep-disordered breathing among middle-aged adults," New England Journal of Medicine vol. 328(17), pp. 1230–1235, 1993.

Yu. S; Cheng. J; , "A Wireless Physiological Signal Monitoring System with Integrated Bluetooth and Wi-Fi Technologies," Engineering in Medicine and Biology Society, 2005. IEEE-EMBS 2005. 27th Annual International Conference of the , vol., no., pp.2203-2206, 17-18 Jan. 2006

Zhang, X., Tao, X., "Smart textiles: Passive smart," June 2001 pp. 45-49; "Smart textile: Active smart," July 2001, pp. 49-52; "Smart textiles: Very smart," August 2001, pp. 35-37, Textile Asia.

Zhou.P., Sui.F., Zhang.A., Wang.F., Li.G., "Music therapy on heart rate variability," Proc. BMEI 3rd International Conference on Biomedical Engineering and Informatics,3, 965-968(2010).

Pratyush Rai received his PhD from University of Arkansas in 2013, where he also received his M.S. in Biomedical Engineering in 2008. He graduated from IIT Madras in 2006 with B Tech. in Biotechnology. His PhD thesis work focused on development of novel textile based nanostructured sensors for detection of biopotential sensing, which are the basis of smart textile sensors for monitoring arrhythmias, EKG, EEG, blood pressure and skin impedance. He has worked on high performance OTFT based flexible sensor electronics, particularly for large scale integrated circuits for sensor arrays. His M.S. work involved development of solution processed organic semiconductor FET based sensors for Myocardial Ischemia detection and development of nano-bio-battery to power these sensors. He is a Research Associate in Department of Electrical Engineering at University of Arkansas. He is the team lead for high performance nanosensor design and fabrication on wearable platforms/textiles for athletes, with emphasis on printed nanosensors on textile. He has authored journal, conference papers, press releases and invention disclosures for the aforementioned technologies.

Sechang Oh received B.S. and M.S. degree in Electrical Engineering from Kyungpook National University, Korea in 1996 and Pohang University of Science and Technology, Korea in 1999. He received his PhD degree in electrical engineering from the University of Arkansas in 2013. From 1999 to 2008, he worked for the LG INNOTEK Co., Ltd., where he was involved in the development of wireless communication modules and electronic devices. He was involved in the development of a wireless network camera using motion detection, audio/video recording, single packaged Wi-Fi module based on LTCC, dual band WiMAX module, Wibro/Wi-Fi combo module, CDMA (KPCS) full module, Wi-Fi mini PCI card, IF SAW

filters, and 915 MHz VCSO during his tenure at LG INNOTEK Co., Ltd., He has 14 pending patents on his research in Korea. Currently, he is a Research Associate in the Department of Electrical Engineering, University of Arkansas, Fayetteville. His research interest includes biomedical nano-sensors and wireless sensor systems for real time monitoring of pathophysiological changes in the body, wireless health monitoring systems, Point-of-Care health diagnostic systems, biomedical pattern recognition, Human Computer Interface, antenna/ RF/mobile system design, energy harvesting for self-powered systems.

Prashanth Shyam Kumar received his M.S. in

Electrical Engineering from the University of Arkansas in 2011 and a Bachelor of Engineering degree in Biomedical Engineering from Manipal University, Karnataka, India in 2008. His M.S. work involved the development of dry electrode based sensors for Electrocardiogram (ECG) measurement and a wireless multisensor system for estimating Blood pressure without a pressure cuff. He is currently working on developing novel techniques to automatically infer healthcare biometrics from minimally intrusive textile nanosensors and applying them to athletics as well as patient care.

Mouli Ramasamy was born in Coimbatore, India,

in 1988. He received the B.E. degree in electronics and communication engineering from the School of engineering, Saveetha University, India, in 2011, and the MSEE degree in electrical engineering from the University of Arkansas, USA, in 2013. He is currently pursuing his doctoral degree in electrical engineering in the University of Arkansas. In 2011, he joined the University of Arkansas as a Visiting Research Scholar. Later in the same year he joined HCL Technologies, India, as a Software Engineer. During his stint as a Software Engineer, he was also involved with the healthcare software research in IIT (Delhi). His current research interests include wearable electronics and healthcare, Point of Care System, Nano-bio-sensors, pattern recognition, electrophysiology of the brain, bio-potential signal processing and Real time patient monitoring. He was the recipient of the Prolific Young Researcher Award from the Signal and Telecommunications department of Southern Railway in 2009. In 2010, he led at a team of 5 in the AUTCUP-Robotic Conference, Iran, to receive the Best Technical Aspect Award.

Robert Harbaugh was born in West York,

Pennsylvania on April 5, 1952. He graduated from high school in Red Lion, Pennsylvania in 1970 and obtained a BS degree from Lebanon Valley College in 1974. Dr. Harbaugh obtained his M.D. from the Pennsylvania State University College of Medicine in 1978 and received his general surgery and neurosurgery training at Dartmouth from 1978-1985. He was appointed Assistant Professor of Surgery (Neurosurgery) at the Dartmouth Medical School in 1985 and progressed to the rank of Professor of Surgery (Neurosurgery) in 1997 and Professor of Radiology in 2001. During his career at Dartmouth, Dr. Harbaugh served as Director of the Dartmouth-Hitchcock Medical Center Cerebrovascular Disease Center from 1994-2003, Director of Cerebrovascular Surgery from 1989-2003, Director of the Neurosurgical Laboratory from 1985-1997 and as acting Residency Program Director from 1996-1997.

In 2003 Dr. Harbaugh returned to Pennsylvania as Professor and Chairman of the Department of Neurosurgery, Neurosurgery Residency Program Director and Professor of Engineering Science and Mechanics at the Pennsylvania State University. He has recently been recognized as a Penn State University Distinguished Professor (Penn State's highest academic honor) and has been chosen to serve as the Director of the new, university-wide, Penn State Institute of the Neurosciences.

Dr. Harbaugh has been an invited speaker in eleven different countries and throughout the United States. His present research interests include clinical trial design, outcomes analysis and quality improvement in neurosurgery and computer modeling of intracranial aneurysms. He maintains a busy clinical practice specializing in cerebrovascular surgery and tumor surgery.

Dr. Harbaugh has edited three books and published more than 230 articles, book chapters and abstracts. He has served on the editorial boards of Neurosurgery, the American Association of Neurological Surgeons Bulletin, Neurosurgery On Call, the Journal of Neurovascular Disease, the Journal of Neuropsychiatry and Clinical Neurosciences and Neurobiology of Aging. Dr. Harbaugh has obtained funding for 13 grant proposals from the NIH, NATO, USDA, industry and foundations. He has two U.S. patent applications.

He is a member of the AANS, CNS, the American Academy of Neurological Surgery, the SNS, the AANS/CNS Section on Cerebrovascular Surgery (SCVS), the AANS/CNS Tumor Section, the American Stroke Association (ASA), the American Heart Association (AHA) Stroke Council, the New England Neurosurgical Society (NENS), the Pennsylvania Neurosurgical Society (PNS) and the American College of Surgeons (ACS). He has held numerous leadership positions in these organizations including Chair of the SNS Membership Committee, Scientific Program Chair for the Academy, Director-at-Large of the AANS Board of Directors, Chairman of the AANS Digital Technology Committee, Chairman of the AANS/CNS Committee for the Assessment of Quality, Chairman of the AANS/CNS Outcomes Committee, Chairman of the AANS/CNS Quality Improvement Workgroup, Chairman of the AANS/CNS Washington Committee and Member of the Executive Committee and Annual Meeting Chairman of the PNS. Dr. Harbaugh is a Fellow of the ACS and the AHA. He served as a member of the Leadership Committee of the AHA Stroke Council, as Chairman of the SCVS from 2002-2003 and President of the NENS from 2001-2003. He is also the President of the NeuroPoint Alliance, Inc. and CHYNA, LLC

Professor Vijay Varadan is currently the Twenty

First Century Endowed Chair in Nano-and Bio-Technology and Medicine, and Distinguished Professor of Electrical Engineering, and Distinguished Professor of Biomedical Engineering (in College of Engineering), and Neurosurgery (in the College of Medicine) at the University of Arkansas. He is also a Professor of Neurosurgery at Penn State University College of Medicine.

He joined the University of Arkansas in January 2005 after serving on the faculty of Cornell University, Ohio State University and Pennsylvania State University for four decades. He is also the Director of the Center of Excellence for Nano-, Micro-, and Neuro-Electronics, Sensors and Systems.

He has concentrated on the design and development of various electronic, acoustic and structural composites, smart materials, structures, and devices including sensors, transducers, Microelectromechanical Systems (MEMS), synthesis and large scale fabrication of carbon nanotubes, NanoElectroMechanical Systems (NEMS), microwave, acoustic and ultrasonic wave absorbers and filters.

He has developed neurostimulator, wireless microsensors and systems for sensing and control of Parkinson's disease, epilepsy, glucose in the blood and Alzheimer's disease. He is also developing both silicon and organic based wireless sensor systems with RFID for human gait analysis and sleep disorders and various neurological disorders.

He is a founder and the Editor-in-Chief of the Journal of Smart Materials and Structures. He is the Editor-in-Chief of the Journal of Nanomedical Science in Engineering and Medicine. He is an Associate Editor of the Journal of Microlithography, Microfabrication and Microsystem. He serves on the editorial board of International Journal of Computational Methods. He has published more than 500 journal papers and 550 conferences proceedings and 17 books. He has 15 patents pertinent to conducting polymers, smart structures,

smart antennas, phase shifters, carbon nanotubes, and implantable device for Parkinson's patients, MEMS accelerometers and gyroscopes. He is a fellow of SPIE, ASME, Institute of Physics, and Acoustical Society of America. He has many visiting professorship appointments in leading schools overseas.